R. & M. No. 3767

R. & M. No. 3767

PROCUREMENT EXECUTIVE, MINISTRY OF DEFENCE

AERONAUTICAL RESEARCH COUNCIL
REPORTS AND MEMORANDA

Calculations of the Steady Conical Flow past a Yawed Slender Delta Wing with Leading-Edge Separation

By D. I. Pullin

Imperial College of Science and Technology

LONDON: HER MAJESTY'S STATIONERY OFFICE
1975
PRICE £3·90 NET

Calculations of the Steady Conical Flow past a Yawed Slender Delta Wing with Leading-Edge Separation

By D. I. Pullin

Imperial College of Science and Technology

Reports and Memoranda No. 3767*
July, 1972

Summary

The author's treatment of the Mangler and Smith vortex-sheet model of leading-edge separation is extended to the calculation of steady conical flow past a yawed slender delta wing. Introducing yaw destroys the symmetry property inherent in the unyawed problem necessitating that the two leading-edge vortex sheets be treated as independent but mutually interacting singularity distributions in the cross-flow plane of the slender-body theory. From the calculations, predictions are obtained of the variation of the principal quantitative flow characteristics—including the two primary vortex core positions and the wing rolling-moment coefficient—with the incidence and yaw parameters. Comparison of these predictions with experimental data is reasonable qualitatively but only fair quantitatively, the discrepancies being attributed to the neglect, in the flow model, of the effects of the secondary separation system on the windward side of the wing. The range of the present calculations is to some extent limited by failure of the solution technique at lower values of the incidence parameter.

* Replaces A.R.C. 33 963

LIST OF CONTENTS

1. Introduction

In recent years, many theoretical studies of the phenomenon of separated flow about unyawed slender delta wings have appeared in technical reports.[1,2,3] This work culminated in that of Smith,[4] who presented the first really adequate approach to the calculation of flows involving leading-edge separation. Following the earlier work of Mangler and Smith,[3] Smith considered a flow model, based on the slender-body theory, in which each of the two spiral vortex sheets representing leading-edge separation are broken up into an outer part, retaining a sheet-like character, and an inner part, the circulation of which is concentrated on to an isolated vortex. He developed an *ad hoc* iterative technique for the numerical treatment of this model and used this scheme to calculate the flow, with leading-edge separation, past an unyawed semi-infinite flat-plate delta wing. Levinsky and Wei[5] have subsequently employed the same method to treat slender bodies formed of combinations of circular/elliptical cones and flat-plate delta wings. Smith[6] has since extended his treatment to deal with leading-edge separation from slender rhombic cones thus calculating for the first time the formation of a free vortex sheet at a leading edge of non zero cross-section angle, while Barsby[7] has used a variation of the Smith approach to investigate the effect of blowing from the leading-edge of a slender delta wing.

Earlier, an alternative model for the treatment of separated flows had been developed by Sacks *et al.*[8] In this approach, the separated shear layers are represented by discrete vortices—shed from the wing leading-edges—which are allowed to convect in an inviscid unsteady flow. This model is suitable for the calculation of non-conical flows but, like all approaches based on the slender-body theory, trailing-edge effects cannot be directly taken into account. Simplified flow models for low aspect-ratio wings in which trailing effects are included, have been presented by Garner and Lehrian,[9] by Polhamus,[10] and by Nangia and Hancock.[11]

More recently, the author[12] has developed an alternative technique to Smith, for the treatment of the slender-body theory vortex-sheet model of conical separated flow. This approach, following Legendre,[1] formulates the general problem for an arbitrary number of vortex sheets, as a system of singular non-linear integro-differential equations. A finite difference representation of these equations, based on the Mangler and Smith vortex-sheet-cut-isolated-vortex model, is constructed, and a Newton–Raphson solution procedure is presented. Some calculated examples with simple leading-edge separation are given.

In all of the above-mentioned work, the slender bodies being treated have incidence to the oncoming stream, but not yaw, thus introducing a plane of symmetry into the problem. A slender conical body with both incidence and yaw may be expected to exhibit a region of approximately conical flow near the apex, and it therefore seems natural to extend the vortex-sheet model to the calculation of such flows. Ribner[13] has treated attached flow past a yawed slender delta wing with and without dihedral, obtaining predictions of the lift and rolling moment, but to the author's knowledge no treatment of the yawed wing problem in which leading-edge separation is included, has yet appeared.

On the experimental side, Fink[14] carried out some preliminary measurements of the pressure distribution on a thin yawed slender delta wing in a region of approximately conical flow. This experimental programme was completed by Harvey,[15] who, in addition to pressure measurements, took detailed flow-field total-head surveys from which the positions of the vortex cores of the windward (attacking edge) and leeward leading-edge vortex systems were obtained. By integration of the wing pressure distribution, he also obtained the local lift and rolling-moment coefficients.

From these experiments it was apparent that yawing the wing strengthened the windward vortex system which moved inboard and closer to the wing surface. Exactly the converse happened to the leeward system.

In the present work, the problem of flow with leading-edge separation past a semi-infinite flat-plate delta wing—with both incidence and yaw—is treated using the inviscid slender-body theory. This allows the construction of a quasi two-dimensional complex velocity potential in the cross-flow plane. The flow is assumed to be conical and flow separation is taken to occur only at the wing 'leading-edges'. Firstly, the set of integro-differential equations for the strength and position of the two vortex sheets which represent the respective separated shear-layer core-systems is derived, and a finite difference representation of these equations is formulated, based on the Mangler and Smith vortex-sheet-cut-isolated-vortex model. A Newton–Raphson iterative procedure is then used to solve the resulting set of non-linear algebraic equations for a range of values of the incidence and yaw parameters.

From the solutions, predictions are obtained of the positions of the vortex core centres of the leeward and windward separation systems, and also of the wing surface-pressure distribution and hence of the wing normal-force and rolling-moment coefficients. Comparison of the variation of these quantities with incidence and yaw, with the experimental data of Harvey[15] is fair, differences being largely attributed to the neglect of the influence of secondary separation on the windward side of the wing.

For an envelope of values of the incidence and yaw parameters, the Newton–Raphson procedure failed to yield solutions of the defining equations. This failure was associated with values of the incidence parameter

in the low part of the range considered, and occurred, in particular, for flow situations for which experimental evidence might lead one to suspect that solutions should exist.

It is perhaps of interest to note here, that solutions obtained for values of the yaw angle greater than half of the wing apex angle represent the calculation of a vortex-sheet from a trailing edge. The general approach to the present problem, including the formulation and solution of the relevant equations, is similar to that adopted in the author's treatment[12] of the unyawed problem.

2. Theory

We consider conical inviscid separated flow about a semi-infinite flat-plate delta wing with both incidence and yaw, in which separation from the leading-edge is represented by free conical surfaces of discontinuity in the velocity potential known as 'vortex-sheets'. The effects of secondary and other separation, which might possibly be incorporated into such a flow model are ignored. The problem is formulated within the slender-body theory of Munk, Jones and Ward, of which the basic assumption is that stream-wise gradients of the flow properties are much smaller than the corresponding gradients normal to the free stream. We are thus restricted to the treatment of delta wings of very small aspect ratio.

2.1. Statement of the Problem

Consider a slender semi-infinite delta wing in uniform stream and choose axes 0–x–y–z fixed in the wing as shown in Fig. 1. The wing lies in the x–y plane such that the x axis bisects its apex angle at 0, and is semi-infinite in the positive x direction. Let δ, which is small, be the half apex angle of the wing and let U be the free-stream velocity inclined at small angles α to the x–y plane and β to the x–z plane. The sense of these angles is taken such that for small α and β, to first order, the components of the free-stream velocity relative to the wing are

$$U, \qquad -\beta U, \qquad \alpha U,$$

in the x, y and z directions respectively.

Then, since the flow is inviscid and irrotational, a velocity potential exists, which, within slender-body theory will be of the form

$$\Phi(x, y, z) = Ux + \phi_0(x, y, z), \tag{1}$$

for small α, β, and where ϕ_0 must satisfy

$$\frac{\partial^2 \phi_0}{\partial y^2} + \frac{\partial^2 \phi_0}{\partial z^2} = 0. \tag{2}$$

The most general solution of equation (2) is

$$\phi_0(x, y, z) = \phi(y, z; x) + g(x, M_0), \tag{3}$$

where M_0 is the free stream Mach number. The first term of equation (3) is a two-dimensional velocity potential in the y–z 'cross-flow' plane in which x appears as a parameter. The second term, $g(x, M_0)$, is a function which appears in the general slender-body theory, but which vanishes for the present case of a flat delta wing.

Figure 2 shows the cross-flow plane at some value of x for which the wing semi-span is $s = Kx$. The cross-section of the wing is represented by $L_1 A L_2 B L_1$, a cut in the y–z plane, and the cross-sections of the leeward and windward vortex sheets by further cuts C_1 and C_2 respectively. The points L_1 and L_2 represent the leading-edges of the slender delta wing being considered. Free-stream-velocity components in the cross-flow plane are shown as $-\beta U$ in the y direction and αU in the z direction. Since the flow is assumed to be conical, the geometry of Fig. 2 will be that for any cross-section $x = \text{const} > 0$, the scale being altered accordingly.

Mangler and Smith[3] have shown that, for conical flow, within the context of slender-body theory, the appropriate conditions which must be satisfied at each point P_j† on C_j, may be written as

† We introduce the convention that if a subscript j appears whose range is unspecified, it is to be taken to be $j = 1, 2$, referring to quantities on the leeward and windward sheets respectively as shown in Fig. 2. In particular P_j represents a point on a vortex sheet.

$$\frac{\partial \phi}{\partial n_j} = -KU\left(\frac{r_j}{s}\right)\sin \chi_j, \tag{4}$$

for the condition that a vortex sheet is a stream surface of the three-dimensional flow, and

$$\Delta\phi_j = \Delta\left(\frac{\partial \phi}{\partial \sigma_j}\right)\left\{r_j \cos \chi_j - s\left(\frac{\partial \phi}{\partial \sigma_j}\right)_m \Big/ KU\right\}, \tag{5}$$

for the condition that the pressure is continuous across the sheet, where

σ_j is the arc length along C_j measured as positive from the appropriate leading edge L_j,

n_j is the normal to C_j as shown in Fig. 2,

Δ is the difference operator across either C_1 or C_2, taken as left–right, where left and right are defined relative to increasing σ_j along the appropriate C_j, $\Delta\phi_j$ for instance, being the jump in the discontinuous velocity potential at P_j,

$\dfrac{\partial \phi}{\partial n_j}$ is the velocity normal to and continuous across C_j, at P_j, and

$\left(\dfrac{\partial \phi}{\partial \sigma_j}\right)_m$ is the mean of the discontinuous tangential velocity at P_j.

The other symbols are as defined in the notation.

Since by equation (2), ϕ is harmonic, it is convenient to introduce a complex velocity potential $W(Z)$, $Z = y + iz$, in the cross-flow plane, such that $\phi = \mathrm{Re}\,(W)$. At infinity in the cross-flow plane, the velocity must approach the appropriate components of the free-stream velocity. Hence we may write, for the form of the velocity potential $W(Z)$ for large Z

$$W(Z) \sim -U(\beta + i\alpha)Z + 0\left(\frac{1}{Z}\right), \tag{6}$$

since there must be no sources or overall circulation in the Z plane.

The problem is thus to find the velocity potential $\phi = \mathrm{Re}\,(W)$, a solution of equation (2) which satisfies

(a) Condition (6) in the Z plane,

(b) Conditions (4) and (5) on C_j, $j = 1, 2$, and

(c) Condition (4) on $L_1 A L_2 B L_1$ (Fig. 2), since the flat-plate delta wing must also be a stream surface of the flow.

2.2. The Integro-Differential Equations for The Yawed Wing Problem

In Ref. 12, the system of integro-differential equations for a number of mutually interacting twin-vortex-sheet systems in an unyawed flow were derived. The symmetry of the problem about the x–z plane was embodied in the form of the equations, and, in particular, in the transformation of the cross-flow plane introduced to facilitate construction of the complex velocity potential. In the present problem, we consider only one pair of vortex-sheets, but the introduction of yaw destroys the symmetry inherent in the unyawed problem, and we must here regard the two leading-edge vortex-sheets as independent surfaces of discontinuity in the flow, whose shape and strength will be determined by the mutual and self interaction of the singularity distributions used to represent them, together with the action of the free stream and the effect of the wing. We now derive the pair of integro-differential equations expressing this interaction by considering the form of the velocity potential which satisfies conditions (a)–(c) outlined at the end of Section 2.1.

Along any curve in the Z-plane, and in particular, at a point $P_j(Z_j)$ (Fig. 2) we may write

$$\left(\frac{\partial \phi}{\partial \sigma_j}\right)_m - i\left(\frac{\partial \phi}{\partial n_j}\right) = \left(\frac{dW}{d\sigma_j}\right) = \left(\frac{dW}{dZ}\right)_{Z_j}\left(\frac{dZ_j}{d\sigma_j}\right). \tag{7}$$

But from conditions (4) and (5) on C_j

$$\left(\frac{\partial\phi}{\partial\sigma_j}\right)_m - i\left(\frac{\partial\phi}{\partial n_j}\right) = \left\{ r_j(\cos\chi_j + i\sin\chi_j) - \frac{\Delta\phi_j}{\Delta\left(\frac{\partial\phi}{\partial\sigma_j}\right)} \right\} \frac{KU}{s}, \tag{8}$$

and combining expressions (7) and (8) gives:

$$KU\left\{\left(\frac{r_j}{s}\right)e^{i\chi_j} - \frac{1}{s}\frac{\Delta\phi_j}{\Delta\left(\frac{\partial\phi}{\partial\sigma_j}\right)}\right\} \Big/ \frac{dZ_j}{d\sigma_j} = \left(\frac{dW}{dZ}\right)_{z_j}. \tag{9}$$

Now for any curve in the Z-plane, $Z_j = Z_j(\sigma_j)$, we have

$$\left.\begin{aligned} \frac{dZ_j}{d\sigma_j} &= e^{i\psi_j} \\ \text{or alternatively} \\ \frac{d\bar{Z}_j}{d\sigma_j} &= e^{-i\psi_j} = 1 \Big/ \left(\frac{dZ_j}{d\sigma_j}\right), \end{aligned}\right\} \tag{10}$$

where ψ_j is the angle between the positive y-direction and the position vector to P_j, as shown for the windward vortex sheet in Fig. 2.

Substituting equation (10) into expression (9) and noting that

$$\Delta\left(\frac{\partial\phi}{\partial\sigma_j}\right) = \frac{\partial(\Delta\phi_j)}{\partial\sigma_j},$$

one obtains

$$KU\left\{\left(\frac{r_j}{s}\right)e^{i(\chi_j-\psi_j)} - \frac{1}{s}\frac{\Delta\phi_j}{\frac{\partial(\Delta\phi_j)}{\partial\sigma_j}\frac{d\sigma_j}{d\bar{Z}_j}}\right\} = \left(\frac{dW}{dZ}\right)_{z_j}. \tag{11}$$

From simple geometrical considerations (Fig. 2), we have

$$\theta_j = \psi_j - \chi_j$$

and thus expression (11) may be written as, at P_j

$$KU\left\{\left(\frac{\bar{Z}_j}{s}\right) - \Delta\phi_j\frac{d(\bar{Z}_j/s)}{d(\Delta\phi_j)}\right\} = \left(\frac{dW}{dZ}\right)_{z_j}, \tag{12}$$

where

$$\left(\frac{\bar{Z}_j}{s}\right) = \left(\frac{r_j}{s}\right)e^{-i\theta_j}.$$

From equation (7), it can be seen that expression (12) represents the mean of the discontinuous complex velocity at P_j.

We now introduce the transformation

$$Z = \frac{1}{2}\left(Z^* + \frac{1}{Z^*}\right), \tag{13}$$

which transforms a circle of radius s, $L_1^*A^*L_2^*B^*L_1^*$ in the Z^*-plane (Fig. 3A), to a slit of width $2s$, $L_1AL_2BL_1$ in the Z-plane, and the curves C_j^* in the Z^*-plane to C_j in the Z-plane.

Working in the Z^*-plane, we can now construct a velocity potential which will satisfy condition (4) on $L_1AL_2BL_1$, by applying the Milne–Thompson circle theorem to the function

$$F(Z^*) = -\frac{U}{2}(\beta + i\alpha)Z^* - \frac{1}{2\pi i}\int_{\Gamma_1}^{0} \log\{Z^* - t_1^*(\Delta\phi_1)\}\, d(\Delta\phi_1) - \frac{1}{2\pi i}\int_{\Gamma_2}^{0} \log\{Z^* - t_2^*(\Delta\phi_2)\}\, d(\Delta\phi_2),$$

and by disregarding a term in the resulting expression which represents an isolated vortex of strength $\Gamma_1 + \Gamma_2$ at $Z^* = 0$, in order to satisfy the required form of $W(Z)$ for large Z in the original cross-flow plane, as expressed by equation (6). Carrying this operation out, we obtain for the complex velocity potential

$$W(Z^*) = -\frac{U}{2}\left\{(\beta + i\alpha)Z^* - (-\beta + i\alpha)\frac{s^2}{Z^*}\right\} - \frac{1}{2\pi i}\int_{\Gamma_1}^{0} \log\left\{\frac{Z^* - t_1^*(\Delta\phi_1)}{Z^* - s^2/\overline{t_1^*}(\Delta\phi_1)}\right\} d(\Delta\phi_1) -$$
$$- \frac{1}{2\pi i}\int_{\Gamma_2}^{0} \log\left\{\frac{Z^* - t_2^*(\Delta\phi_2)}{Z^* - s^2/\overline{t_2^*}(\Delta\phi_2)}\right\} d(\Delta\phi_2), \tag{14}$$

where the first term represents the attached flow, which leads to velocity singularities at L_j in the Z-plane. The factor $1/2$ appears because of the form of the transformation, equation (13). The two integral terms represent the velocity potential at a point Z^* due to the two sheets C_j^*, together with their images $C_j'^*$ in the circle $|Z^*| = s$.

In expression (14) it should be noted that:

(1) The integrals are to be evaluated along C_j^*, $j = 1, 2$ respectively, $t_j^*(\Delta\phi_j)$ representing parametrically, in the integrals, the as-yet unknown shape of C_j^*.

(2) The potential difference $\Delta\phi_j$ across C_j^*, at some point P_j^*, is used in the same sense as in equation (5). It is to be considered as an independent variable along C_j^*. A given value of $\Delta\phi_j$, $|\Gamma_j| \geqslant |\Delta\phi_j| \geqslant 0$ will uniquely define a point P_j^* and will take the same value at corresponding points [through equation (13)] P_j in the Z-plane.

(3) $\Delta\phi_j$ is taken to be Γ_j at L_j^* and zero at the end points of C_j^*. Thus Γ_j is the total circulation around both C_j and C_j^*, at the particular value of x, for which $s = Kx$. It represents the total circulation in the jth separation shear layer at this x-station, and because of the assumed conicality of the flow, Γ_j is linear in x.

Differentiating expression (14) with respect to Z, and evaluating the resulting complex velocity at some point $Z_j^*(\Delta\phi_j)$ on C_j^*, we obtain†

$$\left(\frac{dW}{dZ}\right)_{Z_j} = \left(\frac{dZ^*}{dZ}\right)_{Z_j^*}\left[-\frac{U}{2}\left\{(\beta + i\alpha) + (-\beta + i\alpha)\frac{s^2}{Z_j^{*2}}\right\} -\right.$$
$$- \frac{1}{2\pi i}\int_{\Gamma_1}^{0}\left\{\frac{1}{Z_j^* - t_1^*(\Delta\phi_1')} - \frac{1}{Z_j^* - s^2/\overline{t_1^*}(\Delta\phi_1')}\right\} d(\Delta\phi_2') -$$
$$\left. - \frac{1}{2\pi i}\int_{\Gamma_2}^{0}\left\{\frac{1}{Z_j^* - t_2^*(\Delta\phi_2')} - \frac{1}{Z_j^* - s^2/\overline{t_2^*}(\Delta\phi_2')}\right\} d(\Delta\phi_2')\right]. \tag{15}$$

Note that the whole expression is a function of $\Delta\phi_j$ defining Z_j^* or Z_j. For $j = 1$, the first integral in expression (15) is singular, and for $j = 2$, the second is singular. The integral in each case is interpreted as a Cauchy principle value integral, taking the mean of the two values obtained by approaching Z_j^* from either side of C_j^*.

Combining equations (15) and (12), and introducing the following non-dimensionalising transformations

$$\left.\begin{aligned} \lambda_j &= 1 - \frac{\Delta\phi_j}{\Gamma_j}, \\ \omega_j &= \frac{Z_j}{s} = \xi_j + i\eta_j, \\ \omega_j^* &= \frac{Z_j^*}{s} = \xi_j^* + i\eta_j^* \\ \text{and} \\ \tau_j^* &= \frac{t_j^*}{s} \qquad\qquad j = 1, 2, \end{aligned}\right\} \tag{16}$$

† In carrying out this operation we replace the integration variables $\Delta\phi_j$ in equation (14), by $\Delta\phi_j'$.

we obtain†:

$$\left(\frac{d\omega}{d\omega^*}\right)_{\omega_j^*}\left\{\bar{\omega}_j + (1-\lambda_j)\frac{d\bar{\omega}_j}{d\lambda_j}\right\} = -\tfrac{1}{2}\{(b+ia) - (b-ia)/\omega_j^{*2}\} + \\ + \frac{G_1}{2\pi i}\int_0^1 \left\{\frac{1}{\omega_j^* - \tau_1^*(\lambda_1')} - \frac{1}{\omega_j^* - 1/\bar{\tau}_1^*(\lambda_1')}\right\} d\lambda_1' + \\ + \frac{G_2}{2\pi i}\int_0^1 \left\{\frac{1}{\omega_j^* - \tau_2^*(\lambda_2')} - \frac{1}{\omega_j^* - 1/\bar{\tau}_2^*(\lambda_2')}\right\} d\lambda_2' \\ j = 1, 2, \tag{17}$$

where

$$\omega_j = \frac{1}{2}\left(\omega_j^* + \frac{1}{\omega_j^*}\right), \qquad G_j = \Gamma_j/KUs, \tag{18}$$

$$a = \alpha/K, \qquad b = \beta/K,$$

and

$$K = \tan\delta \simeq \delta, \qquad \text{for small } \delta.$$

Equations (17) together with (18) are a pair of complex simultaneous integro-differential equations for the real and imaginary parts of

$$\omega_j^*(\lambda_j) = \xi_j^*(\lambda_j) + i\eta_j^*(\lambda_j), \qquad 1 \geqslant \lambda_j \geqslant 0,$$

for $j = 1, 2$, where λ_j is the normalized non-dimensional potential difference across either C_j or C_j^*. The parameters a and b, which are to be specified when solving equations (17) and (18), represent incidence and yaw respectively. The parameters G_j are unknowns of the problem and represent the total circulation about C_j or C_j^*. They are made determinate within the mathematical model by applying closure conditions, namely the Kutta conditions, which require that the velocity be finite at the leading edges L_1 and L_2 in the cross-flow plane.

These conditions may be expressed as

$$\left(\frac{dW/KUs}{d\omega^*}\right)_{\omega^* = \omega_{j0}^*} = 0 \qquad j = 1, 2, \tag{19}$$

which by differentiation of equation (14), and application of relations (16), can be written in terms of the flow parameters as

$$a + \frac{G_1}{2\pi}\int_0^1 \left\{\frac{1}{\omega_{j0}^* - \tau_1^*(\lambda_1')} - \frac{1}{\omega_{j0}^* - 1/\bar{\tau}_1^*(\lambda_1')}\right\} d\lambda_1' + \\ + \frac{G_2}{2\pi}\int_0^1 \left\{\frac{1}{\omega_{j0}^* - \tau_2^*(\lambda_2')} - \frac{1}{\omega_{j0}^* - 1/\bar{\tau}_2^*(\lambda_2')}\right\} d\lambda_2' = 0 \\ j = 1, 2, \tag{20}$$

where $j = 1$, $\omega_{10}^* = (-1, 0)$ is the first Kutta condition applied at L_1^*, and $j = 2$, $\omega_{20}^* = (1, 0)$ is the second Kutta condition applied at L_2^*, and (20) are two real equations since the expressions in brackets are real.

It should be noted that, in equations (17) and (20), the incidence and yaw angles appear only in ratio to $K = \tan\delta$. Thus we may regard a and b as similarity parameters of the problem. Solutions of equations (17) and (20) and quantitative properties of these solutions, will therefore be functions of a and b only.

---

† Terms involving a subscript j appearing twice, such as $d\bar{\omega}_j/d\lambda_j$, for example, are to be understood as *not* to be summed.

3. Numerical Treatment

3.1. Finite-Difference Form of the Equations and the Zero-Force Conditions

We now formulate a closed set of non-linear finite difference equations to replace equations (17) and (20), based on the Mangler and Smith vortex-sheet-cut-isolated-vortex model, discussed in detail in Ref. 4. Each sheet C_j^* in the ω^*-plane is broken up into an outer part defined over $\lambda_{jN} \geqslant \lambda \geqslant 0$, and an inner part, $1 \geqslant \lambda > \lambda_{jN}$. The outer part of C_j^* is represented by N discrete points in the ω^*-plane

$$\omega_{jn}^* = \xi_{jn}^* + i\eta_{jn}^* \qquad \begin{matrix} j = 1, 2, \\ n = 1 \ldots, N, \end{matrix} \tag{21a}$$

and the outer part of C_j by N corresponding points in the ω-plane

$$\omega_{jn} = \xi_{jn} + i\eta_{jn} \qquad \begin{matrix} j = 1, 2, \\ n = 1 \ldots, N. \end{matrix} \tag{21b}$$

The discrete values of λ corresponding to expressions (21a) and (21b), we write as

$$\lambda_{jn} = h_n \lambda_{jN}, \qquad \begin{matrix} j = 1, 2, \\ n = 1 \ldots, N, \end{matrix} \tag{21c}$$

where

$$h_N = 1 > h_{N-1} \ldots > h_2 > h_1 > 0,$$

and the h_n are to be specified. Note that λ_{1N} and λ_{2N} are not necessarily equal.

The inner part of C_j^* is represented by an isolated vortex at a point ω_{jN+1}^* and is joined to ω_{jN}^*, the end of the outer part of C_j^*, by a cut in the ω^*-plane, introduced so as to define the potential ϕ unambiguously. This ensures that the velocities induced by the inner part of the sheet on the rest of the flow field are adequately modelled. Corresponding isolated vortices and cuts exist in the ω-plane. The complex velocity $d(W/KUs)/d\omega^*$ is continuous across the cuts but the potential ϕ is not, suffering a discontinuity equal in magnitude to the circulation concentrated at the isolated vortex. Thus, while the outer part of the representation retains its sheet-like character within the model, the inner part does not, any possibility of satisfying equations (17) in some form for $1 > \lambda > \lambda_{jN}$ being discarded. The equivalent points representing $C_j'^*$, the image of C_j^* in the circle $|\omega^*| = 1$, are given by

$$\frac{1}{\overline{\omega_{jn}^*}} = \frac{1}{\xi_{jn}^* - i\eta_{jn}^*} \qquad \begin{matrix} j = 1, 2, \\ n = 1 \ldots, N + 1. \end{matrix} \tag{22}$$

Figure (3B) shows the break-up of C_j^* and $C_j'^*$ for the finite difference representation. Of the total non-dimensional circulation about C_j^*, a fraction λ_{jN} is distributed along the N elements of the outer part, and a fraction $1 - \lambda_{jN}$ will be concentrated at the isolated vortex ω_{jN+1}^*, or equivalently, at ω_{jN+1} in the ω-plane.

We then have $4N + 6$ unknowns given by:

(1) The $N + 1$ real parts ξ_{jn}^*, and the $N + 1$ imaginary parts η_{jn}^*, of ω_{jn}^*, $j = 1, 2$, $n = 1 \ldots, N + 1$, that is $4N + 4$ unknowns, and

(2) The circulations G_j, $j = 1, 2$,

We further choose to introduce an extra degree of freedom by allowing λ_{1N} to be a free parameter (arbitrarily chosen instead of λ_{2N}) while specifying λ_{2N}, giving now $4N + 7$ unknowns, which we represent vectorially by $\boldsymbol{\Omega}$, with components

$$\Omega_l \qquad l = 1 \ldots, 4N + 7,$$

arranged in some arbitrary order, the details of which will not concern us here.

To find a suitable $\boldsymbol{\Omega}$ representing a solution of the problem for given values of a, b, h_n, $n = 1 \ldots, N$ and λ_{2N},

$4N + 7$ relations involving $\boldsymbol{\Omega}$ are required. $4N$ of these are supplied by satisfying equations (17) in finite difference form along the outer part of the sheet, and 2 more are given by the finite difference form of equations (20). Four more relations are supplied by satisfying conditions of zero total force on each cut-isolated vortex system in the ω-plane. This is introduced so as to make the inner part of the model force free in lieu of one in which the inner part retains its sheet-like character, each element being force and moment free. One final condition introduced, is that the sum of the two moments due to the pressure difference on the cuts $\omega_{jN+1} - \omega_{jN}$, is zero.

It should be emphasised that this 'zero-moment condition' has no significance in the sense that the zero force condition has for the inner part of each sheet. It is associated with the parameter λ_{1N}, and unlike the zero force conditions, it need not be incorporated into the model to obtain realistic solutions. We could for example specify λ_{1N} and drop the moment condition since it is unlikely that the main physical parameters of the problem —the sheet shape near the leading edge, the positions of the isolated vortices and the circulations—will depend strongly upon it. Nevertheless since the moment condition does ensure that overall, the fluid in the vicinity of the wing is moment free, we choose to include it.

We satisfy a finite difference form of equations (17) at points in the ω^* plane defined by

$$\left.\begin{aligned} \omega^*_{jn,n-1} &= \tfrac{1}{2}(\omega^*_{jn} + \omega^*_{jn-1}) \\ \text{and} \qquad \lambda_{jn,n-1} &= \frac{\lambda_{jN}}{2}(h_n + h_{n-1}) \qquad \begin{matrix} j = 1, 2, \\ n = 1 \ldots, N \end{matrix} \end{aligned}\right\}. \tag{23}$$

Corresponding points $\omega_{jn,n-1}$ in the ω plane are given through equation (18). The left-hand side of (17) is replaced by a two point differentiation rule along C_j and the integrals on the right-hand side in $\lambda_{jN} \geqslant \lambda \geqslant 0$ are evaluated at points given by equations (23) using the trapezoidal rule (ignoring the singularity), that part for $\lambda > \lambda_{jN}$ being given by the velocity field due to an isolated vortex. Thus a finite difference representation of equations (17) can be written as

$$\begin{aligned} H_{jn}(\boldsymbol{\Omega}) = &- \left(\frac{d\omega}{d\omega^*}\right)_{\omega^*_{jn,n-1}} \left\{ \overline{\omega_{jn-1}} \left(\frac{h_n - 1/\lambda_{jN}}{h_n - h_{n-1}} \right) - \overline{\omega_{jn}} \left(\frac{h_{n-1} - 1/\lambda_{jN}}{h_n - h_{n-1}} \right) \right\} - \\ &- \tfrac{1}{2}\{(b + ia) + (-b + ia)/\omega^{*2}_{jn,n-1}\} + \\ &+ \frac{G_1}{2\pi i} \sum_{m=0}^{N+1} A_{1m} \left\{ \frac{1}{\omega^*_{jn,n-1} - \omega^*_{1m}} - \frac{1}{\omega^*_{jn,n-1} - 1/\overline{\omega^*_{1m}}} \right\} + \\ &+ \frac{G_2}{2\pi i} \sum_{m=0}^{N+1} A_{2m} \left\{ \frac{1}{\omega^*_{jn,n-1} - \omega^*_{2m}} - \frac{1}{\omega^*_{jn,n-1} - 1/\overline{\omega^*_{2m}}} \right\} = 0, \\ & \qquad\qquad j = 1, 2, \qquad n = 1 \ldots, N, \end{aligned} \tag{24}$$

where

$$\begin{aligned} A_{l0} &= h_1 \lambda_{lN}, \\ A_{lm} &= (h_{m+1} - h_{m-1}) \frac{\lambda_{lN}}{2} \qquad m = 1 \ldots, N - 1, \\ A_{lN} &= (1 - h_{N-1}) \frac{\lambda_{lN}}{2}, \end{aligned}$$

and

$$A_{lN+1} = 1 - \lambda_{lN} \qquad l = 1, 2.$$

Expression (24) is complex and represents $4N$ equations, $2N$ real and $2N$ imaginary. The terms $(d\omega/d\omega^*)\omega^*_{jn,n-1}$, $\overline{\omega_{jn}}$ and $\overline{\omega_{jn-1}}$ in equation (24) can be evaluated in terms of $\overline{\omega^*_{jn}}$ and $\overline{\omega^*_{jn-1}}$ through equation (18).

In equations (20) for the Kutta conditions, the integrals over the outer part of the sheets may be written as

$$\frac{G_l}{2\pi} \sum_{m=1}^{N} \int_{\lambda_{lm-1}}^{\lambda_{lm}} \left\{ \frac{1}{\omega^*_{j0} - \tau^*_l} - \frac{1}{\omega^*_{j0} - 1/\overline{\tau^*_l}} \right\} d\lambda, \tag{25}$$

for both $l = 1, 2$ in each case of equation (20), $j = 1, 2$.

The integral for $j = l$, $m = 1$ in the above has a singularity (not of the Cauchy principle value type) at the leading-edge L_j, where $\lambda_j = 0$ and $\tau_j^* = 1/\overline{\tau_j^*} = \omega_{j0}^*$. From solutions of equation (17) valid near L_j, that is, for small λ_j, it can be shown that the sheet shape is given by

$$\tau_j^* = \omega_{j0}^* + A_j\lambda^{\frac{1}{2}} + iB_j\lambda + 0(\lambda^{1+\mu}), \tag{26}$$

where $\mu > 0$ and where A_j and B_j are real constants that depend on the overall flow. Substitution of this expression into the first integral for $j = l$ in expression (25) yields

$$\frac{G_j}{2\pi}\int_0^{\lambda_{j1}} \left\{\frac{1}{\omega_{j0}^* - \tau_j^*} - \frac{1}{\omega_{j0}^* - 1/\overline{\tau_j^*}}\right\} d\lambda$$

$$= \frac{G_j h_1 \lambda_{jN}}{\pi} \frac{4}{2\omega_{j0}^* - (\omega_{j1}^* + \overline{\omega_{j1}^*})} - \frac{1}{2\omega_{j0}^*} + 0(\lambda_{j1}^{1+\gamma})$$

$$\text{where} \quad \gamma > 0. \tag{27}$$

The other integrals in equation (25) are evaluated using the trapezoidal rule and thus the first Kutta condition $j = 1$, $\omega_{10}^* = (-1, 0)$ in equations (20) can be replaced by, dropping the term of $0(\lambda_{j1}^{1+\gamma})$ in equation (27)

$$Q_1(\boldsymbol{\Omega}) = a + \frac{G_1 h_1 \lambda_{1N}}{\pi} \frac{4}{2\omega_{10}^* - (\omega_{11}^* + \overline{\omega_{11}^*})} - \frac{1}{2\omega_{11}^*} +$$

$$+ \frac{G_1}{2\pi}\sum_{m=1}^{N+1} A'_{1m}\left\{\frac{1}{\omega_{10}^* - \omega_{1m}^*} - \frac{1}{\omega_{10}^* - 1/\overline{\omega_{1m}^*}}\right\} +$$

$$+ \frac{G_2}{2\pi}\sum_{m=0}^{N+1} A_{2m}\left\{\frac{1}{\omega_{10}^* - \omega_{2m}^*} - \frac{1}{\omega_{10}^* - 1/\overline{\omega_{2m}^*}}\right\} = 0 \tag{28a}$$

where

$$A'_{11} = (h_2 - h_1)\frac{\lambda_{1N}}{2} \qquad A'_{1m} = A_{2m}, \qquad m \geqslant 2.$$

The second Kutta condition, $j = 2$, $\omega_{20}^* = (1, 0)$ can be written in a similar manner to equation (28a), with the subscripts 1 and 2 reversed. We represent this condition, symbolically as

$$Q_2(\boldsymbol{\Omega}) = 0. \tag{28b}$$

From considerations of the three-dimensional flow, Smith[4] shows that the conditions of zero force on each cut and isolated vortex may be written as

$$\lim_{\omega \to \omega_{jN+1}} \left\{\frac{d(W/KUs)}{d\omega} - \frac{G_j(1 - \lambda_{jN})}{2\pi i}\frac{1}{\omega - \omega_{jN+1}}\right\} - \overline{2\omega_{jN+1}} + \overline{\omega_{jN}} = 0 \tag{29}$$

$$j = 1, 2,$$

where the limit represents the velocity at ω_{jN+1} in the cross-flow plane, if the isolated vortex were not present. When this limit has been taken and the resulting integrals replaced by trapezoidal rule quadratures, equation (29) can be written in finite difference form as

$$E_1(\boldsymbol{\Omega}) = \left[-\tfrac{1}{2}\{(b + ia) + (-b + ia)/\omega_{1N+1}^{*2}\} + \right.$$

$$+ \frac{G_1}{2\pi i}\left\{\sum_{m=0}^{N}\frac{A_{1m}}{\omega_{1N+1}^* - \omega_{1m}^*} - \sum_{m=0}^{N+1}\frac{A_{1m}}{\omega_{1N+1}^* - 1/\overline{\omega_{1m}^*}}\right\} +$$

$$\left. + \frac{G_2}{2\pi i}\sum_{m=0}^{N+1} A_{2m}\left\{\frac{1}{\omega_{1N+1}^* - \omega_{2m}^*} - \frac{1}{\omega_{1N+1}^* - 1/\overline{\omega_{2m}^*}}\right\}\right] \left(\frac{d\omega}{d\omega^*}\right)_{\omega_{1N+1}^*} +$$

$$+ \frac{G_1(1 - \lambda_{1N})}{4\pi i}\left\{\frac{d}{d\omega^*}\left(\frac{d\omega^*}{d\omega}\right)\right\}_{\omega_{1N+1}^*} - \overline{2\omega_{1N+1}} + \overline{\omega_{1N}} = 0, \tag{30a}$$

for the first zero-force condition, together with a similar equation with the subscripts 1 and 2 reversed for the second zero-force condition

$$E_2(\mathbf{\Omega}) = 0, \tag{30b}$$

where the A_{jm}, $j = 1, 2$, $m = 1 \ldots, N + 1$, are as in equations (24), and equations (30) are 4 equations since equations (30a) and (30b) both have real and imaginary parts.

We now derive the condition of zero total moment on the two cuts $\omega_{jN+1} - \omega_{jN}$ in the ω plane. Within the context of slender-body theory, the pressure coefficient at some point in the three-dimensional flow about the flat plate delta wing is given by (Ref. 4)

$$C_P = 2\left(y\frac{\partial\phi}{\partial y} + z\frac{\partial\phi}{\partial z} - \phi\right)\Big/ Ux - \left\{\left(\frac{\partial\phi}{\partial y}\right)^2 + \left(\frac{\partial\phi}{\partial z}\right)^2\right\}\Big/ U^2 + \alpha^2 + \beta^2. \tag{31}$$

Now since both $\partial\phi/\partial y$ and $\partial\phi/\partial z$ are continuous across the cuts $\omega_{jN+1} - \omega_{jN}$, there will exist a constant pressure difference across each cut given by, from equation (31)

$$\begin{aligned}\Delta p_j &= \tfrac{1}{2}\rho U^2 \Delta C_{P_j} = -\frac{\rho U \Delta\phi_j}{x} \\ &= -\frac{\rho U \Gamma_j(1 - \lambda_{jN})}{x}.\end{aligned} \tag{32}$$

The x-wise moment per unit length in the x-direction, of this pressure difference about Z_{jN+1} in the Z plane can thus be written as

$$\begin{aligned}D_j &= \tfrac{1}{2}\Delta p_j(Z_{jN+1} - Z_{jN})(\overline{Z}_{jN+1} - \overline{Z}_{jN}) \\ &= -\frac{\rho U}{2x}\Gamma_j(1 - \lambda_{jN})(Z_{jN+1} - Z_{jN})(\overline{Z}_{jN+1} - \overline{Z}_{jN}) \\ &\qquad\qquad j = 1, 2.\end{aligned} \tag{33}$$

Then since the total force per unit length in the x direction on each cut-isolated-vortex system is zero, taking moments about the origin of the Z-plane yields the condition that the sum of the x-wise moments in the fluid, near the wing, due to the existence of the two cut-isolated-vortex systems is zero, viz:

$$\sum_{j=1}^{2} D_j = 0, \tag{34}$$

which can be transformed to non-dimensional variables using relations (16), to give

$$M(\mathbf{\Omega}) = \sum_{j=1}^{2} G_j(1 - \lambda_{jN})(\omega_{jN+1} - \omega_{jN})(\overline{\omega_{jN+1}} - \overline{\omega_{jN}}) = 0, \tag{35}$$

where (35) is one real equation.

For the unyawed case ($b = 0$), equation (35) is satisfied by $G_1 = -G_2$, $\lambda_{1N} = \lambda_{2N}$ and $\omega_{1n} = -\overline{\omega_{2n}}$, $n = N, N + 1$. This is automatically satisfied by symmetry in the formulations of the unyawed problem in References 4 and 12.

Equations (24), (28), (30) and (35) are the $4N + 7$ equations involving the $4N + 7$ unknowns of the problem. We represent these equations symbolically, their various real and imaginary parts assumed separated (which is actually not explicitly necessary for the solution procedure used herein), as

$$f_k(\mathbf{\Omega}) = 0, \qquad k = 1 \ldots, 4N + 7, \tag{36}$$

the order of k in respect to equations (24), (28), (30) and (35) being chosen in some arbitrary but convenient way.

3.2. Solution Procedure

For the present work, equations (36) were solved for fixed values of $h_1 \ldots h_N$ and λ_{1N}, for a range of values of a and b, by a Newton–Raphson technique previously developed by the author.[12] This method is a single iteration procedure and amounts to a full linearisation of equations (36) about some known approximation to a desired solution. A full outline of this method is given in Ref. 12. Only sufficient details are given here to indicate its present application.

Each iteration of the above-mentioned scheme involves first the calculation of a $(4N + 7) \times (4N + 7)$ matrix, the components of which are

$$F_{kl} = \frac{\partial f_k}{\partial \Omega_l} \qquad \begin{matrix} k = 1 \ldots, 4N + 7, \\ l = 1 \ldots, 4N + 7, \end{matrix} \tag{37}$$

and the subsequent solution of a set of $4N + 7$ linear equations of the form

$$\sum_{l=1}^{4N+7} F_{kl}(\mathbf{\Omega}^p)\, \delta\Omega_l^{p,p+1} = -f_k(\mathbf{\Omega}^p) \qquad k = 1 \ldots, 4N + 7. \tag{38}$$

In equations (38), the f_k and the F_{kl} are evaluated at a pth approximation, say $\mathbf{\Omega}^p$, to a solution of equations (36). The $\delta\Omega_l^{p,p+1}$ are the unknowns of the linear system, from which a $(p + 1)$th approximation given by

$$\Omega_l^{p+1} = \Omega_l^p + \delta\Omega_l^{p,p+1} \qquad l = 1 \ldots, 4N + 7,$$

can be constructed. Repeated calculation of matrices (37) and solution of equations (38) (by a standard method), for $p = 1, 2 \ldots$, yields a sequence of approximations which should converge to a satisfactory solution of equations (36).

The derivatives $\partial f_k / \partial \Omega_l$ are determined by direct differentiation of equations (24), (28), (30) and (35) with respect to the various components of $\mathbf{\Omega}$. With regard to the real variables G_1, G_2 and λ_{1N}, the differentiation is straightforward. With regard to the components of $\mathbf{\Omega}$ which represent the real and imaginary parts of $\omega_{jn}^* = \xi_{jn}^* + i\eta_{jn}^*$, $n = 1 \ldots, N + 1$, $j = 1, 2$, the required derivatives are found by differentiation with respect to ω_{jn}^* and $\bar{\omega}_{jn}^*$, and use of the relations

$$\text{and} \qquad \begin{aligned} \frac{\partial f_k}{\partial \xi_{jn}^*} &= \begin{Bmatrix} \mathrm{Re} \\ \mathrm{Im} \end{Bmatrix} \left[\frac{\partial V}{\partial \omega_{jn}^*} + \frac{\partial V}{\partial \bar{\omega}_{jn}^*} \right] \\ \frac{\partial f_k}{\partial \eta_{jn}^*} &= \begin{Bmatrix} \mathrm{Re} \\ \mathrm{Im} \end{Bmatrix} \left[i \left(\frac{\partial V}{\partial \omega_{jn}^*} - \frac{\partial V}{\partial \bar{\omega}_{jn}^*} \right) \right] \end{aligned} , \tag{39}$$

where f_k for some value of k, is either the real or imaginary part of the complex equation

$$V(\mathbf{\Omega}) = 0, \tag{40}$$

V being any of H_{jn}, $n = 1 \ldots, N$, Q_j, E_j, $j = 1, 2$ or M in equations (24), (28), (30) and (35).

3.3. Choice of Numerical Parameters

Solutions of equations (36) will be of the form

$$\Omega_l = \Omega_l(a, b; h_1, h_2 \ldots, h_N, \lambda_{2N}), \qquad l = 1 \ldots, 4N + 7, \tag{41}$$

The work of Smith[4,6] on the unyawed problem, and the author's own experience indicates that solutions will not depend strongly on λ_{2N}, provided that sufficient of the outer part of the sheet is represented in a sheet-like manner. Sufficient in this context may be taken to mean:

(a). That at least that part of the sheet which extends from the leading edge of the wing to a point where it may be considered that the spiral 'rolling up' process has properly begun, is included in the representation of the outer part.

(b). That enough of the sheet near the wing leading-edge is treated in a sheet-like manner to ensure that the velocity field in this region is adequately modelled.

Smith uses a geometrical variable—namely the polar angle θ (in Ref. 4) taken around the isolated vortex in the transformed plane—to specify the extent of the outer part of the sheet and concludes, from numerical experiment, that the choice $\theta_{max} = 157$ degrees (maximum polar angle) gives an adequate representation. In the author's treatment of the unyawed problem[12] for the flat plate, calculations were made for both $\lambda_{1N} = \lambda_{2N} = 0{\cdot}45$, $N = 20$ and $\lambda_{1N} = \lambda_{2N} = 0{\cdot}195$, $N = 10$ (roughly equivalent to $\theta_{max} = 157$ degrees) which confirmed Smith's conclusion.

Hence, for the present work, $N = 10$ points were chosen on the outer part of the sheet and λ_{2N} was chosen as $\lambda_{2N} = 0{\cdot}2$, that is, 20 per cent of the total circulation on the windward system is distributed along the sheet and 80 per cent is concentrated at the isolated vortex. The fraction of the total circulation distributed on the sheet in the leeward system is, of course, an unknown of the problem.

The values of h_n chosen were as follows:

TABLE 1

n	1	2	3	4	5	6	7	8	9	10
h_n	0·01	0·04	0·10	0·25	0·375	0·50	0·625	0·75	0·875	1·0

3.4. Computational Details; Range of Solutions

A Fortran IV computer progam (not included in the present report) was written embodying the solution procedure outlined above, in which the various numerical parameters of the problem—including an initial approximation—could be input as data. Using this program, approximate numerical solutions to equations (36) were found, with the above values of $h_1 \ldots, h_N$ and λ_{2N}, over a range of values of a and b. For given values of a and b, the solution procedure was terminated and a solution considered to be found, when an iterate, say $\mathbf{\Omega}^p$, was obtained which satisfied the condition

$$\frac{1}{4N+7} \sum_{k=1}^{4N+7} |f_k(\mathbf{\Omega}^p)| \leqslant 10^{-8}. \tag{42}$$

It is believed (though it is not proven herein), that when condition (42) is satisfied, a solution to equation (36) has been found accurate to four significant figures in each of the components of $\mathbf{\Omega}$. This is considered to be more than sufficiently accurate given the limitations of the mathematical flow model, and the accuracy of the available experimental data. The conclusion that this degree of accuracy has been obtained was reached by observing that there was, in general, no change in the fifth significant figure of components of successive iterates, say $\mathbf{\Omega}^p$ and $\mathbf{\Omega}^{p+1}$, when (42) had been satisfied by $\mathbf{\Omega}^p$. Usually 4–5 iterations were required to reduce the l.h.s. of equation (42) from 0(1) to $0(10^{-8})$, requiring about 10 seconds of CDC-6600 computing time. Often convergence was so fast in the later iterations that the l.h.s. of equation (42) was reduced to values several orders of magnitude lower than 10^{-8}.

Calculations were made for values of a up to 3·0, and values of b up to 2·0 along lines of constant a or b in the a–b plane. Starting approximations were obtained from solutions for $b = 0$, that is, from solutions to the unyawed problem. Solutions with yaw were then found by increasing b by intervals of 0·1 or smaller (where necessary), at fixed values of $a = 0{\cdot}5$, 1·0, 1·5, 2·0, 2·5 and 3·0. From solutions obtained along the $a = 3{\cdot}0$ line in the a–b plane, further solutions were found by decreasing a by intervals of 0·1 at constant values of b given by $b = 0{\cdot}5$, 1·0, 1·5 and 2·0. In this way, a grid of solutions was obtained in the region $0 \leqslant b \leqslant 2{\cdot}0$, $0 \leqslant a \leqslant 3{\cdot}0$, of the a–b plane.

However, as stated in the introduction, it was found that at lower values of a, over the whole range of b, the Newton–Raphson scheme diverged, failing to yield solutions of the finite-difference equations. The lowest value of a for a given value of b, for which solutions could be obtained, was found to be given approximately by

$$a = 0{\cdot}15 + 0{\cdot}4b. \tag{43}$$

Thus, in a significant part of that region of the a–b plane, in which solutions were sought, none could be found. This phenomenon is discussed further in Section 4.2.

4. Results and Comparison with Experiment

Table 2 gives a summary of the significant numerical parameters obtained from solutions of the defining equations. It lists the positions ξ_{jN+1}, η_{jN+1}, $j = 1, 2$, of the two isolated vortices in the ω plane, the total circulations $G_j, j = 1, 2$, of the two sheet-isolated vortex systems, and the fraction λ_{1N} of the total circulation distributed along the sheet in the leeward system, for values of a and b separated by 0·5. Also shown are the normal-force coefficient C_N/K^2, calculated by the method of residues [equation (A-9), Appendix], and the rolling moment coefficient $C_{\mathscr{L}}/K^2$ calculated by numerical integration of the first moment of the pressure coefficient across the wing surface, equation (A-13).

4.1. Vortex Sheet Shapes

Vortex sheet shapes and isolated vortex positions are shown, for the values of a and b indicated, in Figs. 4a, 5a and 6a for the leeward system and in Figs. 4b, 5b and 6b for the windward system. They may be regarded as typical graphical representations of solutions obtained to the finite difference equations and serve to illustrate the principal features of, and in particular the extent of typical vortex sheet shapes in relation to the positions of the associated isolated vortices.

The sheet shapes presented were constructed by drawing smooth lines through the plotted solution points $\xi_{jn}, \eta_{jn}, n = 1 \ldots, N, j = 1, 2$. A typical distribution of these points along the outer part of the sheet is shown in Figs. 6a and 6b, where they are plotted for $a = 1{\cdot}5$, $b = 2{\cdot}0$. In Figs. 4a and 4b, the sheet shapes for $a = 0{\cdot}5$ and $b = 0{\cdot}95$ represent the solution for the largest value of b (for $a = 0{\cdot}5$) which could be obtained before the aforementioned failure of the iteration scheme occurred. For $a = 1{\cdot}0$ (Figs. 5a and 5b), failure occurred for values of b only slightly larger than 2·0, but for $a = 1{\cdot}5$ (Figs. 6a and 6b), the solution range could be extended considerably beyond $b = 2{\cdot}0$. A general comment regarding Figs. 4 to 6 worth mentioning here, is that for $b = 0$, the twin-vortex-sheet system exhibits, quite naturally, the symmetry property about the η axis expected for zero yaw.

It would seem, from Figs. 4b, 5b and 6b, that the geometrical extent of the outer part of the windward vortex sheet is adequate even though only 20 per cent of the total windward circulation is distributed along it, 80 per cent being concentrated at the isolated vortex. In each of these figures, the extent of the outer part of the sheet increases with b indicating a movement of circulation towards the asymptotic centre of the system. As b increases at constant a, there appears to be a tendency for the whole windward sheet-vortex system to move closer to the wing surface, while the overall windward circulation G_2 (the variation of which with a and b, is shown in Fig. 10b), increases quite strongly. At higher values of a than those depicted in Figs. 4b, 5b and 6b, the tendency is not so much a movement toward the wing, as a movement inboard toward the wing centre-line. This is illustrated by the variation of the position of the isolated vortex, as shown by the heavy lines in Fig. 9.

The outer part of the leeward vortex sheet is not so well represented geometrically as that of the windward sheet. From Figs. 4a, 5a and 6a, it can be seen that, as b increases, the distance between the free end of the sheet and the isolated vortex increases, and for higher values of b, it might well be argued that insufficient† of the outer part of the sheet is represented, to satisfy condition (a) in Section 3.3. The effect of this on the calculated position of the leeward vortex is that it is possibly too far to leeward, the velocity inducing effect of the 'missing part' of the sheet, in the vicinity of the vortex being a component to windward. This is illustrated in Fig. 5a, where, for $a = 1{\cdot}0$, $b = 1{\cdot}0$, a leeward sheet and vortex position, calculated with λ_{1N} held fixed at $\lambda_{1N} = 0{\cdot}20$, is shown. The solution for the same a and b, in which the zero-moment condition is applied yields $\lambda_{1N} = 0{\cdot}159$ (Table 2). For $a = 1{\cdot}0$ and $a = 1{\cdot}5$ (Figs. 5a and 6a), as b increases, the isolated vortex approaches more nearly the tangent to the sheet at its free end. Although part of this effect can probably be attributed to the above-mentioned error in the calculation of the vortex position, it is nevertheless believed to be a genuine indication that the sheet (if it were continued) is becoming more tightly wound, geometrically, about its asymptotic centre.

The main effect, of increasing b, on the position of the leeward sheet and vortex can be seen to be a marked movement to leeward. For $b > 1$, the wing leeward edge must be considered to be a trailing edge, since for these cases $\beta > \delta$. Thus in solutions calculated for $b > 1$ the leeward vortex sheet can be interpreted as one emanating from a trailing edge, and the overall flow, as that in the tip region of a very highly forward swept wing with a pointed tip of small apex angle.

---

† Note, however, that at values of b near $b = 2{\cdot}0$, the calculated value of λ_{1N} increases sharply (Table 2), which means that quite a substantial fraction of the total leeward circulation is distributed along the outer part of the sheet.

In the present study, through the assumptions used in obtaining equation (26) and its subsequent inclusion in equation (28) for the finite difference formulation of the Kutta conditions; we have constrained both vortex sheets to separate in an outboard direction, tangentially to the wing undersurface at their respective leading edges. Barsby[16] however, has suggested that under certain conditions a vortex sheet need not necessarily separate in this manner but may do so tangentially to the upper wing surface in a configuration consistent with a flow onto the leading edge. In this case, the separation point would lie inboard of the leading edge. Hence the most plausible explanation for the failure of the solution scheme is that for low values of a, our present model of separation is untenable for the windward vortex sheet which should in fact separate as Barsby suggests. This would be consistent with the appearance of inflection points in the windward sheet shape (*see* Figs. 4b, 5b and 6b) near the leading edge, close to failure. To incorporate Barsby's separation model into the present formulation for values of a, say below those given by equation (43), an alternative to the present treatment of the singularity at the windward leading edge would be required.

4.2. Isolated Vortex Positions; Circulation

4.2.1. *Calculated vortex positions* The heavy lines in Figs. 7 and 9 show the variation of the calculated position of the leeward and windward isolated vortices respectively, and also depict a comparison of the calculated values with Harvey's[15] experimentally determined core positions. Figure 8 shows a similar comparison of the calculated vortex positions on the leeward side with the results of an experiment carried out by the author.

For $b > 0$, there is no longer symmetry of the two vortex-sheet-isolated-vortex systems about $\xi = 0$. As b increases at a fixed value of a, Figs. 7 or 8 show that the leeward isolated vortex moves upwards away from the wing surface and towards, and eventually outboard of the leeward leading edge. This movement represents a general trend for all values of a. It is associated with a weakening of the leeward system which may be seen in Fig. 10a as a decrease in the magnitude of the total circulation G_1 with b at constant a. However, while the rate of movement of the vortex position with b appears to increase with increasing b, the rate of change of $|G_1|$ seems to decrease to near zero. Thus, at large yaw, the leeward vortex moves rapidly outboard with increasing b while the overall leeward circulation remains nearly constant. The main effect on the position of the leeward vortex, of increasing a at constant b, is a marked vertical movement and a corresponding increase in $|G_1|$.

The effect of relaxing the zero-moment condition, on the position of the leeward isolated vortex, is illustrated in Fig. 8 where the dash–dotted line shows its variation with b for $a = 1{\cdot}0$, obtained from solutions calculated with λ_{1N} held constant at $\lambda_{1N} = 0{\cdot}20$. Differences between vortex positions given by this curve and those given by the heavy line (for $a = 1{\cdot}0$), begin to become significant at values of b somewhat less than $b = 1{\cdot}0$, where the calculated value of λ_{1N} associated with the zero moment condition begins to differ appreciably from $\lambda_{1N} = 0{\cdot}2$ (*see* Table 2). Where this value exceeds 0·2, the vortex positions given by the heavy line are to be preferred, and where it is less than 0·2, those given by the dot–dashed line will be more accurate. The effect of holding λ_{1N} fixed, on the windward vortex position, is too small to be illustrated graphically. The effect on the normal-force and rolling-moment coefficients was found to amount to, except at very large yaw, a fractional change of less than 1 per cent.

On the windward side of the wing, at high values of a, there can be discerned (Fig. 9) a strong inboard movement of the vortex, without much variation in the height, as b increases at constant a. For intermediate incidence ($a = 1{\cdot}5$, 1·0) the inboard movement is less marked and there is a definite downward movement towards the wing surface. The variation of the vortex position with b is not very systematic for these values of a and is completely haphazard for $a = 0{\cdot}5$, over the small range of b for which solutions could be obtained with $N = 10$, $\lambda_{2N} = 0{\cdot}20$.

As a decreases at constant b, the vortex path can be seen to move outboard and downwards towards the windward leading edge, the loci for all values of b converging as a decreases, until failure of the iteration scheme is encountered. The extremities of the heavy lines in Figs. 7, 8 and 9 at the lower values of a represent the first onset of failure for the values of b indicated. The appropriate values of a are given by equation (43). To verify that this failure was not a numerical effect associated with, say, the particular numerical parameters chosen, some solutions for $N = 8$, $\lambda_{2N} = 0{\cdot}15$ were obtained for values of a below 1·0. In general, for a fixed b, the iteration scheme first diverged at about the same value of a for the $N = 10$, $\lambda_{2N} = 0{\cdot}2$ cases. However, whereas for $a = 0{\cdot}5$, no $N = 10$ solutions could be found for $0{\cdot}08 < b < 0{\cdot}5$ (although solutions could be obtained for $0{\cdot}5 \leqslant b \leqslant 0{\cdot}95$), $N = 8$ solutions could be found for all $0{\cdot}0 \leqslant b \leqslant 0{\cdot}95$. The vortex loci for these $N = 8$ solutions are shown in Figs. 7, 8 and 9 as dotted lines. On the leeward side, the $N = 8$ isolated vortex positions are

reasonably close to the $N = 10$ ones, except near the point of solution failure, but on the windward side, there is significant difference, the loci for both values of N being quite unrealistic.

4.2.2. *Present experiment.* In Ref. 15 Harvey presents maps of the total head surveys (Figs. 7 to 15) he obtained for various values of the incidence and yaw angles α and β and also a summary graph showing the variation of the leeward and windward vortex cores, taken as the positions of the respective total head absolute minima. Unfortunately there seems to be a discrepancy between the core positions that can be inferred from the total head maps and those presented in the summary graph. Discussion with Dr. Harvey led to the conclusion that the summary graph—Fig. 16 in Ref. 15—in fact gives the correct experimental determination of the vortex cores, the total head maps being incorrect due to scale errors in the plotting process. Regrettably the original total head data has been lost.

To verify that Harvey's summary graph indeed gives the correct core positions, and to determine core positions for some values of a and b which were not covered in Harvey's work, a further experiment was carried out by the author, in the 5 ft × 4 ft low speed wind tunnel at Imperial College. This was performed with the same delta wing ($\delta = 10$ degrees) used by Harvey. Experimental conditions, and in particular the Reynolds number ($Re \simeq 6{\cdot}1 \times 10^5$, based on distance from the wing apex) were generally similar to those of Ref. 15.

The leeward primary core positions were determined by searching for the absolute total head minima in the flow field, using a Kiel tube mounted on a Deiser traverse gear, for yaw angles of $\beta = 0$, 5, 10, 15 and 20 degrees at each of 3 values of the incidence, $\alpha = 5$, 10 and 15 degrees. Measurements were made only on the leeward side of the wing as it is believed that the effect of secondary separation on the windward side is so strong at higher values of b, as to make the extra data that might be obtained not worthwhile in relation to the present work.

4.2.3. *Comparison with experiment.* Comparison of the calculated leeward vortex positions with the experimental† results of Harvey (Fig. 7) and of the author‡ (Fig. 8) is fair and is similar to that obtained by Smith[4,6] for unyawed flow. As b increases and the primary vortex core moves past the leeward leading-edge, the leeward secondary separation system diminishes in size and influence, eventually vanishing completely. One might therefore expect that comparison with experiment would improve, the higher the value of b. From Figs. 7 and 8 it can be seen that this is not the case, the measured core-positions being, in general, rather inboard of the calculated positions of the isolated vortex.

As was noted in Section 4.1, as b increases, the geometric extent of the outer part of the leeward vortex-sheet becomes less adequate, the probable effect on the calculated vortex position being an error to leeward. Since this is just the direction of the general theoretical–experimental discrepancy, we might perhaps interpret it as being the result of the improvement in the aptness of the flow model with increasing b (diminishing secondary separation), being to some extent offset by a slight worsening in the sufficiency of the present numerical representation.

It can be seen from Fig. 9 that comparison with experiment on the windward side of the wing is not good and in fact worsens with increasing yaw. In general the height of the vortex core is well predicted but the lateral position is not, the calculated values being much too far inboard of the measured ones. These discrepancies are more likely attributable to the neglect of the windward secondary separation shear-layer core system, the size of which, as noted by Harvey,[15] increases with increasing yaw. The fact that the windward core position is not well predicted will, of course, through the mutual coupling of the velocity inducing effects of the leeward and windward circulatory systems, introduce errors into the calculated position of the leeward isolated vortex. However, since the two systems are fairly remote from each other, this effect is thought to be small.

4.2.4. *Circulation.* Figures 10a and 10b show the variation of the total circulation of the leeward and the windward systems, G_1 and G_2 respectively, with b at constant a. That $|G_1|$ decreases with increasing b has been previously noted. The circulation of the windward system, on the other hand, can be seen to increase quite strongly with increasing b, the rate of increase rising with both a and b. Thus for intermediate and large yaw, the windward circulatory system is much the stronger of the two. These trends are confirmed qualitatively by Harvey's[15] observations concerning the variation in strength of the absolute minima of his total head surveys, with α and β.

---

† In Figs. 7, 8 and 9 similarly flagged symbols of different type (different incidence) represent experimental results at the same yaw angle.

‡ Note that the present experimental leeward primary core positions, as they are based on one measurement only, must be considered to be less reliable than those of Harvey, which were inferred from detailed total head surveys.

4.3. Wing Surface Pressure Distributions

The pressure coefficient—expressed as C_p/K^2 so as to be a function of a, b and $\xi = y/s$ only†—was calculated, for various a and b, at discrete points along the upper and lower wing surfaces using equations (A-1) to (A-5) in the Appendix. Figures 11 to 16 show graphically the calculated pressure distributions, for the values of a and b indicated and compare them with measured distributions obtained by Fink[14] and Harvey[15] in regions of approximately conical flow.

It can be seen in Figs. 11 to 16 that there appears to be a relative shift in the vertical scales of the calculated and measured distributions amounting to about 1·5 units of C_p/K^2. The present theoretical distributions for $b = 0$ are in good agreement with those of Ref. 4, calculated for unyawed flow. Furthermore the centreline pressure coefficients on the underside of the wing are for all cases, slightly larger than the corresponding attached flow values

$$\left[\frac{C_p}{K^2}\right]_{\text{ATT},\omega=(0,0^-)} = a(a+2),$$

which is consistent with the additional velocity inducing effect of vortex sheets present in the separated flow. It is therefore believed that the experimental distributions presented in Refs. 14 and 15 are slightly in error, a circumstance which is thought to have arisen due to a static-pressure gradient which probably existed in the flow between the tunnel axis and the static-pressure tappings on the tunnel wall. This, of course, would not affect estimates of local lift and rolling moments obtained from them, which was the primary objective of the experiment.

Fig. 11, for $a = 0{\cdot}5$, Figs. 12 and 13, for $a = 1{\cdot}0$ and Figs. 14 to 16 for $a = 1{\cdot}5$ clearly indicate the effect of yaw on the calculated wing-surface pressure distributions. As b increases from zero, the distributions lose their symmetry about $\xi = 0$. The windward upper-surface suction peak follows the windward isolated vortex inboard and increases in strength, corresponding to the rise in the total circulation of the windward system and the slight downward movement of the isolated vortex. On the leeward side, the general effect is quite the opposite, the suction peak collapsing rapidly (as b increases), and moving outboard toward the leading edge in sympathy with the calculated movement of the isolated vortex, and the decrease in magnitude of the circulation of the leeward system. No pressure distribution is presented for which the leeward vortex is actually outboard of the leading edge, but for such cases the leeward suction peak vanishes completely.

Comparison of calculated and experimental distributions is generally quite good along the lower surface of the wing and fair on the leeward upper surface. The large discrepancies which exist between theory and experiment on the windward upper surface, and which increase with increasing yaw, are believed to be due to the effects of secondary separation. The presence of this phenomenon influences the pressure distribution on the windward side of the wing directly, in that it causes a reduction in the size of the suction peak and inhibits pressure recovery between the primary vortex core and the wing leading edge. An indirect effect is that it displaces the primary core inboard. Overall the effect might be described as a 'flattening and broadening' of the windward suction peak. That the calculated suction peak is much too strong and is too far outboard is consistent with the discrepancies, previously noted, between the calculated and measured primary vortex positions. That the predicted shape is manifestly incorrect may be explained by the absence of the modifying effects of secondary separation as described above.

As the influence of secondary separation on the leeward side of the wing diminishes (with increasing b), comparison with experiment improves significantly and in fact the shape of the small leeward suction peak is quite well predicted for the higher values of b in Figs. 11c, 12b and 16.

It is interesting to note that at higher values of a and b, the calculated pressure distributions resemble more nearly those appropriate to a two-dimensional wing at incidence in a uniform stream. This is not surprising since with the present formulation, the limiting case

$$a \to \infty$$

$$b \to \infty$$

$$a/b \to \text{Const} = \tan(\gamma), \text{ say,}$$

corresponds to a two-dimensional flow (at incidence γ) with both leading- and trailing-edge separation. Of course, for stability reasons it is unlikely that such a flow could exist.

---

† Integrals of the zeroth and first moments of $\Delta C_p/K^2$ about $\xi = 0$, being the normal-force and rolling-moment coefficients respectively, will thus only be functions of a and b.

4.4. Normal-Force Coefficient

Equation (A-9) gives the complex lateral force coefficient $(C_Y + iC_N)/K^2$ for the entire wing vortex-sheet-isolated-vortex separated-flow system. Since the wing has no thickness, and since there are no leading-edge-suction forces acting, the y-wise force on the wing must necessarily be zero. Because, however, of small residual forces acting in the fluid (due largely to the finite difference modelling of the integro-differential equations), the overall y-wise force will not vanish. For the same reason, the overall normal-force coefficient obtained from the imaginary part of equation (A-9), will differ from that obtained by numerical evaluation of equation (A-10), the integral of the pressure difference across the wing surface. In the present calculations, the magnitude of the real part of equation (A-9) was always less than 0·5 per cent of the imaginary part, and the fractional difference between the imaginary part, and numerical evaluation of integral (A-10) (using a 5 point rule), was always less than 1·5 per cent and generally less than 1 per cent.

The lift in attached flow is given by the first term of equation (A-9)

$$\left[\frac{C_N}{K^2}\right]_{\text{ATT}} = 2\pi a,$$

and is independent of yaw.

Fig. 17 shows the variation of the imaginary part of $(C_Y + iC_N)/K^2$ with b for various values of a. Also shown are experimental values obtained in Ref. 15 from integration of measured pressure distributions. These values actually represent local normal-force coefficients, but have been corrected to give overall coefficients by assuming that the flow is conical. They therefore exclude trailing-edge effects.

It can be seen from Fig. 17 that the calculated effect of yaw is to increase the separated-flow lift, the rate of increase increasing with both a and b. Harvey's experimental data shows an initial decrease in the overall lift, with increasing yaw, which is not predicted by the present calculations, and a subsequent increase. It is difficult to say whether or not this experimental trend is genuine, although there is no reason to doubt it. Quite possibly it is a result, direct or otherwise, of the change in state of the secondary separation systems with yaw, or it could perhaps be a thickness effect. We may conclude that although the details of the pressure distribution are not well predicted on the windward upper surface, the normal-force coefficient is reasonably well predicted, the regions of under and over prediction of the pressure coefficient, balancing in contribution thereto.

4.5. Rolling-Moment Coefficient

For separated flow, the rolling-moment coefficient $C_{\mathscr{L}}/K^2$ cannot be evaluated by the method of residues (*see* Appendix) and in the present work was calculated by numerical evaluation of a span-wise integral of the first moment of the pressure difference across the wing surface, equation (A-13). Fig. 18 shows the variation of $C_{\mathscr{L}}/K^2$ with b for various values of a. The dotted lines give the attached-flow rolling moment

$$[C_{\mathscr{L}}/K^2]_{\text{ATT}} = -\frac{\pi}{3}ab,$$

obtained by Ribner.[13] As was stated in Section 4.1, for $b > 1$, the leeward wing edge becomes, in fact, a trailing edge, at which it is necessary that the flow satisfy a Kutta condition. Since this is impossible without free circulation, the attached flow has no meaning for $b > 1$, and the dotted lines (in Fig. 18) are therefore terminated at $b = 1$.

Fig. 18 indicates that in general both the attached and separated flow rolling-moment coefficients† increase either with b at constant a or vice-versa. However, for $a = 3{\cdot}0$, after an initial increase with b, the rolling-moment decreases for values of b greater than about 1·5. In general, the difference between the predicted attached and separated flow rolling-moments (for $b < 1$) can be seen to be significant, but not large. Thus although the separated flow considerably alters the wing pressure distribution from that obtained in attached flow, it produces rather smaller fractional changes in the rolling moment than it does in the lift. This may be interpreted as meaning that as b increases at constant a, both the attached- and separated-flow pressure distributions change—from the corresponding distribution at zero yaw—in roughly the same manner, even though they differ quantitatively and qualitatively from each other.

---

† The sense of positive rolling-moment is indicated in Fig. 1.

In Fig. 19, the rolling-moment coefficient plotted as $C_{\mathscr{L}}/(K^2 b)$ is compared with Harvey's experimental values obtained as the first moment of the measured pressure distribution about $\xi = 0$. For $a = 0{\cdot}5$, the comparison is quite good over the range for which solutions could be obtained. At higher a the experimental values generally lie between those predicted for the attached and separated flow. For the separated flow, the largest contribution to the rolling-moment will come from the windward suction-peak region of the wing, and since it is here that the upper surface pressure coefficient is most poorly predicted, it is not surprising that there is large discrepancy between theory and experiment. Since the windward suction peak is calculated to be rather too far outboard, we might expect that the magnitude of the rolling moment might be over-predicted, as is the case for $a = 1{\cdot}0$ and $a = 1{\cdot}5$. The reasonable comparison with experiment obtained for $a = 0{\cdot}5$ must be regarded as fortuitous.

5. Conclusion

Numerical calculations have been made of the conical inviscid flow, with leading-edge separation, past a yawed slender delta wing. The Newton–Raphson iterative technique employed yielded satisfactory solutions to the finite difference equations over ranges of the incidence and yaw parameters, but diverged, failing to do so in a region of the parameter space associated with lower values of the incidence.

For non-zero yaw, comparison of the calculated flow properties with experiment was generally no worse than for zero yaw, there being two notable exceptions, namely the position of the windward primary vortex core and the shape and strength of the associated pressure suction peak on the windward upper surface of the wing. The large theoretical–experimental discrepancies which were found to exist for these quantities were attributed to the increasing influence (with increasing yaw) of the secondary separation system, the effects of which were not included in the flow model.

There was good qualitative agreement between theory and experiment, both of which indicate that increasing the yaw angle:

(a) strengthens the windward primary vortex core which moves inboard and slightly downwards,
(b) weakens the leeward core which moves markedly outboard of the wing centre line and upwards,
(c) causes an increase in strength of the pressure suction peak on the windward upper surface of the wing, and a decrease in that on the leeward upper surface,
(d) produces appreciable increase in the normal-force coefficient only at large yaw, and
(e) induces a rolling-moment on the wing, not very much larger than that predicted by attached flow theory.

It seems probable that the incorporation of Barsby's separation model at the windward leading edge would lead to solutions in the incidence-yaw range for which the present approach fails.

Acknowledgements

The author wishes to thank Dr. J. K. Harvey for his supervision of this research and for his help and guidance in the preparation of this report.

While engaged in this work, the author was supported by a University of Sydney Post-Graduate Travelling Research Scholarship.

LIST OF SYMBOLS

a	$= \alpha/K$, incidence parameter
A_j	Coefficient in expression for vortex-sheet shape near a leading edge, *see* equation (26)
A_{lm}	Coefficient in trapezoidal rule quadrature as defined for equations (24)
$\mathscr{A}_{-1}$	Coefficient of Z^{-1} in expansion of W for large Z
b	$= \beta/K$, yaw parameter
B_j	coefficient in expression for vortex-sheet shape near a leading edge, *see* equation (26)
C_j	Denotes cross-section of jth vortex-sheet in the Z-plane
C_j^*	Transformed shape of C_j in the Z^*-plane
$C_j'^*$	Image of C_j^* in the circle $\lvert Z^*\rvert = s$
C_P	Pressure coefficient
C_N	Normal-force coefficient (z direction)
C_Y	Side-force coefficient (y direction)
$C_{\mathscr{L}}$	Rolling-moment coefficient
$\left[\frac{C_N}{K^2}\right]_{\text{ATT}}$	$\frac{C_N}{K^2}$ in attached flow
$\left[\frac{C_{\mathscr{L}}}{K^2}\right]_{\text{ATT}}$	$\frac{C_{\mathscr{L}}}{K^2}$ in attached flow
$\mathscr{C}_{-1}$	Coefficient of ω^{-1} in expansion of W/KUs for large ω
D_j	x-wise moment acting on jth cut, *see* equation (33)
E_j	$= 0$, symbolic representation of jth zero-force condition [equations (30)]
f_k	$= 0$, symbolic representation of kth equation, in equations (36)
F	Function used in constructing the complex velocity potential in the Z^*-plane
F_{kl}	Matrix coefficient defined in equation (37)
g	Function which appears in the slender-body theory, *see* equation (3)
G_j	$= \Gamma_j/KUs$, nondimensional circulation about the jth vortex-sheet
h_n	Quantity defined in equation (21c)
H_{jn}	$= 0$, symbolic representation of finite difference form of equations (17) at j–nth point
Im	Imaginary part
K	$= \tan \delta$
l	x-distance from apex, *see* equation (A-6)
L_j	Denotes jth leading-edge in the Z-plane
L_j^*	Point to which L_j is transformed, in the Z^*-plane
$\mathscr{L}$	Rolling moment
$\mathscr{L}_{\text{ATT}}$	Rolling moment in attached flow
M	$= 0$, symbolic representation of zero-moment condition [equation (35)]
M_0	Free-stream Mach number
N	Normal force

LIST OF SYMBOLS (continued)

p	Static pressure
P_j	Point on C_j in Z-plane
P_j^*	Point on C_j^* in Z^*-plane
Q_j	$= 0$, symbolic representation of Kutta conditions [equations (28)]
r_j	Scalar distance of P_j from the origin of the Z-plane
Re	Real part
s	Local wing semi-span
t_j^*	Sliding point on the jth vortex-sheet in the Z-plane [*see* equation (14)]
U	Free-stream speed
V	*see* equation (40)
W	Complex velocity potential
x, y, z	Rectangular cartesian co-ordinates, fixed on the wing
Y	Total side (y-wise) force acting on wing plus vortex-sheets
Z	Complex variable in the cross-flow plane
Z_j	A value of Z on the jth vortex-sheet
Z^*	Complex variable in the transformed plane
Z_j^*	A value of Z^* on the jth vortex-sheet
α	Incidence angle of the wing
β	Yaw angle of the wing
γ	Exponent defined for equation (27)
Γ_j	Circulation about jth vortex-sheet
δ	Semi-apex angle of the wing
Δ	Difference operator across vortex-sheet, *see* equations (4) and (5)
$\Delta\phi_j$	Potential difference across jth vortex-sheet
Δp_j	Pressure difference across jth cut in cross-flow plane
ΔC_{P_j}	Pressure-coefficient difference across jth cut
η, η_j, η_{jn}	$=$ Im (ω), Im (ω_j), Im (ω_{jn}) respectively
$\eta^*, \eta_j^*, \eta_{jn}^*$	$=$ Im (ω^*), Im (ω_j^*), Im (ω_{jn}^*) respectively
θ_j	Angle in cross-flow plane, *see* Fig. 2
λ_j	$= 1 - \Delta\phi_j/\Gamma_j$, non-dimensional potential difference across jth vortex-sheet
λ_{jn}	Value of λ_j at ω_{jn} or ω_{jn}^*
$\lambda_{jn,n-1}$	Value of λ_j defined in equations (23)
μ	Exponent defined for equation (26)
ξ, ξ_j, ξ_{jn}	$=$ Re (ω), Re (ω_j), Re (ω_{jn}) respectively
$\xi^*, \xi_j^*, \xi_{jn}^*$	$=$ Re (ω^*), Re (ω_j^*), Re (ω_{jn}^*) respectively
ρ	Free-stream density
σ_j	Arc length along C_j [*see* equations (4) and (5)]

τ_j^*	$= \frac{t_j^*}{s}$
ϕ	Quasi two-dimensional velocity potential
ϕ_0	Slender-body theory perturbation potential
χ_j	Angle in cross-flow plane, *see* Fig. 2
Φ	Complete velocity potential
ψ_j	Angle in the cross-flow plane, *see* Fig. 2
ω	$= Z/s$, non-dimensional complex variable in the cross-flow plane
ω_j	A value of ω on the jth vortex-sheet
ω_{jn}	Complex co-ordinate of the nth point on the jth vortex-sheet, in the ω-plane
$\omega_{jn,n-1}$	Point to which $\omega^*_{jn,n-1}$ is transformed, in the ω-plane
ω^*	$= Z^*/s$, non-dimensional complex variable in the transformed plane
ω_j^*	A value of ω^* on the jth vortex sheet
ω_{jn}^*	Complex co-ordinate of the nth point on the jth vortex sheet in the ω^*-plane
$\omega^*_{jn,n-1}$	Midpoint of ω^*_{jn} and ω^*_{jn-1}, defined by equations (23)
$\mathbf{\Omega}$	Vectorial representation of the unknowns of equations (36)
Ω_l	lth component of $\mathbf{\Omega}$
$\mathbf{\Omega}^p$	pth approximation to a solution of equations (36)
Ω_l^p	lth component of $\mathbf{\Omega}^p$
$\delta\Omega_l^{p,p+1}$	$= \Omega_l^{p+1} - \Omega_l^p$

Subscripts

j	Refers to a quantity on a vortex-sheet, $j = 1$, leeward sheet; $j = 2$, windward sheet
k	kth equation in equations (36)
l, m	Dummy subscripts in summation terms; m also denotes the mean value across a vortex sheet
n	Refers to nth point on a vortex-sheet
N	Number of points on the outer part of a vortex-sheet

REFERENCES

No.	*Author(s)*	*Title, etc.*
1	R. Legendre	Écoulement au voisinage de la pointe avant d'une aile à forte flèche aux incidences moyennes. 8th Int. Cong. Th. Appl. Mech. Istanbul (1952). Rech. aéro., No. 30 (1952) and Rech. aéro., No. 31 (1953).
2	C. E. Brown and W. H. Michael ..	On slender delta wings with leading-edge separation. N.A.C.A. Tech. Note 3430, April 1955. *J. Aero. Sci.* 21, 690–694 and 706 (1954).
3	K. W. Mangler and J. H. B. Smith ..	A theory of the flow past a slender delta wing with leading-edge separation. R.A.E. Rep. Aero 2593 (1957). *Proc. Roy. Soc. A.*, 251, 200–217 (1959).
4	J. H. B. Smith	Improved calculations of leading-edge separation from slender delta wings. R.A.E. Technical Report 66070 (1966). *Proc. Roy. Soc. A.*, 306, 67–90 (1968).
5	E. S. Levinsky and M. H. Y. Wei ..	Non-linear lift and pressure distribution on slender conical bodies with strakes at low speeds. N.A.S.A. CR-1202, October 1958.
6	J. H. B. Smith	Calculations of the flow over thick, conical, slender wings with leading-edge separation. A.R.C. R. & M. 3694 (1971).
7	J. E. Barsby	Calculations of the effect of blowing from the leading-edges of a slender delta wing. A.R.C. R. & M. 3692 (1971).
8	A. H. Sacks, R. E. Lundberg and C. W. Hanson	A theoretical investigation of the aerodynamics of slender wing-body combinations exhibiting leading-edge separation. N.A.S.A. CR-719, March 1967.
9	H. C. Garner and D. E. Lehrian ..	Non-linear theory of steady forces on wings with leading-edge separation. A.R.C. R. & M. 3375 (1963).
10	E. C. Polhamus	A concept of the vortex lift of sharp-edge delta wings, based on a leading-edge suction analogy. N.A.S.A. TN D-3767, December 1966.
11	R. K. Nangia and G. J. Hancock ..	A theoretical investigation for delta wings with leading-edge separation at low speeds. A.R.C. C.P. 1086 (1968).
12	D. I. Pullin	A method for calculating inviscid separated flow about conical slender bodies. Aeronautical Research Laboratories (Australia) Aerodynamics Report 140 (1973)

13 H. S. Ribner .. .. .. The stability derivatives of low-aspect-ratio triangular wings at subsonic and supersonic speeds.
N.A.C.A. Tech. Note 1423, September 1947.

14 P. T. Fink .. .. Some early experiments on vortex separation. Part III. Further experiments with 20 deg. delta wings.
A.R.C. R. & M. 3489 (1957).

15 J. K. Harvey .. .. Some measurements on a yawed slender delta wing with leading-edge separation.
A.R.C. R. & M. 3160 (1958).

16 J. E. Barsby .. .. Private communication (1972).

17 A. H. Sacks .. .. Aerodynamic forces, moments, and stability derivatives for slender bodies of general cross section.
N.A.C.A. Tech. Note 3283, November 1954.

APPENDIX

Calculation of the Pressure Coefficient, Normal Force and Rolling Moment

In this appendix, the expressions used to calculate the wing pressure coefficient and the lift and rolling-moment coefficients, are derived.

A.1. Pressure Coefficient

For conical inviscid irrotational flow about a flat-plate delta wing, the slender-body theory prediction of the pressure coefficient is given by (Ref. 4)

$$\frac{C_P}{K^2} = 2\left(y\frac{\partial\phi}{\partial y} + z\frac{\partial\phi}{\partial z} - \phi\right)\Big/ K^2Ux - \left\{\left(\frac{\partial\phi}{\partial y}\right)^2 + \left(\frac{\partial\phi}{\partial z}\right)^2\right\}\Big/ K^2U^2 + a^2 + b^2. \tag{A-1}$$

Note that the pressure coefficient is a quadratic function of the velocity components. Hence while solutions of equation (2) and the derived velocity fields may be superposed [since equation (2) is linear], pressure coefficients and lift and rolling-moment coefficients, in general, may not be obtained by superposition.

It is easily verified that the various terms of equation (A-1) may be expressed in terms of the complex velocity potential W, and the mapping $\omega(\omega^*)$, as follows

$$\left\{\left(\frac{\partial\phi}{\partial y}\right)^2 + \left(\frac{\partial\phi}{\partial z}\right)^2\right\}\Big/ K^2U^2 = \left|\frac{d(W/KUs)}{d\omega^*}\frac{d\omega^*}{d\omega}\right|^2, \tag{A-2}$$

and

$$\left(y\frac{\partial\phi}{\partial y} + z\frac{\partial\phi}{\partial z} - \phi\right)\Big/ K^2Ux = -2\,\mathrm{Re}\left[\frac{W}{KUs} - \omega\frac{d(W/KUs)}{d\omega^*}\frac{d\omega^*}{d\omega}\right]. \tag{A-3}$$

The last three terms of equations (24) (Section 3.1) give the present representation of the complex velocity $d(W/KUs)/d\omega^*$, evaluated at a point $\omega^*_{jn,n-1}$ on a vortex sheet in the ω^* plane. By replacing $\omega^*_{jn,n-1}$ in these terms by ω^*, we obtain an expression for the complex velocity at a general point in the ω^* plane:

$$\begin{aligned}\frac{d(W/KUs)}{d\omega^*} = &-\tfrac{1}{2}\{(b + ia) + (-b + ia)/\omega^{*2}\} + \\ &+ \frac{G_1}{2\pi i}\sum_{m=0}^{N+1} A_{1m}\left\{\frac{1}{\omega^* - \omega^*_{1m}} - \frac{1}{\omega^* - 1/\overline{\omega^*_{1m}}}\right\} + \\ &+ \frac{G_2}{2\pi i}\sum_{m=0}^{N+1} A_{2m}\left\{\frac{1}{\omega^* - \omega^*_{2m}} - \frac{1}{\omega^* - 1/\overline{\omega^*_{2m}}}\right\},\end{aligned} \tag{A-4}$$

where the A_{lm}, $l = 1, 2$ are as in equations (24).

The associated expression for the complex potential W/KUs is obtained by integration of (A-4) with respect to ω^*, which yields

$$\begin{aligned}W/KUs = &-\tfrac{1}{2}\{(b + ia)\omega^* - (-b + ia)/\omega^*\} + \\ &+ \frac{G_1}{2\pi i}\sum_{m=0}^{N+1} A_{1m}\log\left\{\frac{\omega^* - \omega^*_{1m}}{\omega^* - 1/\overline{\omega^*_{1m}}}\right\} + \\ &+ \frac{G_2}{2\pi i}\sum_{m=0}^{N+1} A_{2m}\log\left\{\frac{\omega^* - \omega^*_{2m}}{\omega^* - 1/\overline{\omega^*_{2m}}}\right\}\end{aligned} \tag{A-5}$$

Using equations (A-1) to (A-5), the pressure coefficient can be evaluated at a point in the fluid, and in particular, at a point on the wing surface, provided that suitable branches of the logarithms appearing in equation (A-5) are chosen.

A.2. Normal Force

Sacks,[17] using the slender-body theory, derives expressions for the overall forces and moments acting on a slender body in a generalised state of motion by considering various integrals of the pressure around contours adjacent to the body cross section in the cross-flow plane. In these expressions, where possible, contour integrals involving analytic functions of the complex variable in the cross-flow plane are obtained. These integrals are treated by expanding the contour to infinity and applying the method of residues. Although only attached flows (i.e. those without vortex sheets) are considered in Ref. 17 the arguments used and equations derived therein should be applicable to separated flow problems, provided that the contours considered surround the vortex sheets as well as the body, in the cross-flow plane.

From equation (45) of Ref. 17, the complex lateral force, acting up to a station $x = l$ on a flat plate delta wing with incidence and yaw, in a steady uniform stream may be written as

$$Y + iN = 2\pi\rho U\{\mathscr{A}_{-1}\}_{x=l}, \tag{A-6}$$

where $\mathscr{A}_{-1}$ is the coefficient of Z^{-1} in the expansion for the appropriate complex potential† W, at large Z. The complex lateral force coefficient, when divided by K^2, can be expressed as

$$\frac{C_Y}{K^2} + i\frac{C_N}{K^2} = \frac{Y + iN}{\frac{1}{2}\rho U^2 K^2 sl} \tag{A-7}$$

where $s = Kl$. Hence from equations (A-6) and (A-7) we may write

$$\frac{C_Y}{K^2} + i\frac{C_N}{K^2} = 4\pi\mathscr{C}_{-1} \tag{A-8}$$

where $\mathscr{C}_{-1} = \mathscr{A}_{-1}/(KUs^2)$ is the coefficient of ω^{-1} in the expansion of W/KUs for large ω. Note that equation (A-8) is valid for either attached or separated flow.

For the present problem, $\mathscr{C}_{-1}$ can be evaluated using equations (A-5) and (18) (from Section 2.2), yielding for the overall complex lateral force coefficient

$$\frac{C_Y}{K^2} + i\frac{C_N}{K^2} = 2\pi\left[ia + \frac{G_1}{2\pi i}\sum_{m=0}^{N+1} A_{1m}\left\{\frac{1}{\overline{\omega^*_{1m}}} - \omega^*_{1m}\right\} + \frac{G_2}{2\pi i}\sum_{m=0}^{N+1} A_{2m}\left\{\frac{1}{\overline{\omega^*_{2m}}} - \omega^*_{2m}\right\}\right]. \tag{A-9}$$

The first term on the r.h.s. of equation (A-9) may be interpreted as the linear lateral force due to the attached flow, which, in fact, turns out to be independent of the yaw angle. The summation terms represent the lift due to the separated flow, which depends implicitly, through the solution points ω^*_{jn}, $j = 1, 2$, $n = 1 \ldots, N + 1$, on the incidence and yaw parameters.

Alternatively, the normal-force coefficient may be obtained by integration of the pressure coefficient over the wing upper and lower surface. Because of the conicality of the flow, this integral may be reduced to one along the wing cross section in the cross-flow plane, viz:

$$\frac{C_N}{K^2} = \frac{1}{2}\int_{-1}^{1} \frac{\Delta C_P}{K^2}\, d\xi, \tag{A-10}$$

where ΔC_P is the pressure-coefficient difference, lower surface minus upper surface, across the wing.

A.3. Rolling Moment

Sacks also derives expressions for the rolling-moment acting on a slender body with a generalised motion, namely equation (52) of Ref. 17. However, for the present case, the integrals appearing in this equation can only be evaluated by the method of residues if the initial contour taken about the wing (and vortex sheets,

† Note that in Ref. 17, wing fixed axes are chosen on the moving body such that, at infinity, the lateral velocity components are zero. The different choice of axes for the present work will have no effect on the coefficient $\mathscr{A}_{-1}$—merely adding a term linear in Z to the general form of the velocity potential used by Sacks—and thus the expressions derived in Ref. 17 will be directly applicable to the present case.

if any) has mirror symmetry about the y and z axes. For separated flow, the presence of vortex sheets will mean that there can be no such symmetry, necessitating the use of other methods in the evaluation of the separated-flow rolling-moment.

For attached flow, however, the required symmetry exists (for the present problem), and in this case, equation (52) of Ref. 17 reduces to

$$\mathscr{L}_{\mathrm{ATT}} = -\frac{2\pi\rho K^4 U^2 l^3}{3} \operatorname{Im}[(b + ia)\mathscr{C}_{-1}], \tag{A-11}$$

where $[\mathscr{L}]_{\mathrm{ATT}}$ is the attached-flow rolling-moment and where $\mathscr{C}_{-1}$ is as defined for equation (A-8). Using the expression

$$\left[\frac{C_{\mathscr{L}}}{K^2}\right]_{\mathrm{ATT}} = \frac{\mathscr{L}_{\mathrm{ATT}}}{\rho K^2 U^2 s^2 l},$$

and noting that for attached flow we have

$$\mathscr{C}_{-1} = \frac{ia}{2},$$

we obtain for the attached-flow rolling-moment coefficient

$$\left[\frac{C_{\mathscr{L}}}{K^2}\right]_{\mathrm{ATT}} = -\frac{\pi ab}{3}. \tag{A-12}$$

This result agrees with that obtained by Ribner.[13]

The rolling-moment coefficient for separated flow can be evaluated by a wing-surface integration of the first moment of the pressure about the x axis. Reduction of this integral to one across the wing-span in the cross-flow plane leads to

$$\frac{C_{\mathscr{L}}}{K^2} = -\frac{1}{6}\int_{-1}^{1} \frac{\Delta C_P}{K^2}\xi \, d\xi, \tag{A-13}$$

where $\xi = (y/s)$. In equation (A-13), ΔC_P is as for (A-10). A positive $C_{\mathscr{L}}/K^2$ acts in the sense indicated in Fig. 1. As with equation (A-10), equation (A-13) can be evaluated numerically by a standard method.

TABLE 2

Principal Solution Parameters

$N = 10, \lambda_{2N} = 0{\cdot}20$

a	b	ξ_{1N+1}	η_{1N+1}	G_1	λ_{1N}	ξ_{2N+1}	η_{2N+1}	G_2	$\frac{C_N}{K^2}$	$\frac{C_{\mathscr{M}}}{K^2}$
0·5	0·0	−0·808	0·118	−2·081	0·200	0·808	0·118	2·081	4·586	0·000
0·5	0·5	−0·849	0·162	−1·649	0·131	0·815	0·097	2·469	4·622	−0·349
0·5	0·95	−0·949	0·232	−1·237	0·152	0·815	0·088	2·841	4·807	−0·660
1·0	0·0	−0·704	0·249	−4·610	0·200	0·704	0·249	4·610	10·94	0·000
1·0	0·5	−0·770	0·314	−3·854	0·210	0·673	0·210	5·383	11·11	−0·668
1·0	1·0	−0·950	0·415	−3·177	0·159	0·675	0·182	6·109	11·77	−1·317
1·0	1·5	−1·226	0·510	−2·862	0·190	0·672	0·169	6·884	13·09	−1·882
1·0	2·0	−1·583	0·613	−2·885	0·321	0·662	0·162	7·768	14·92	−2·245
1·5	0·0	−0·660	0·352	−7·563	0·200	0·660	0·352	7·563	18·65	0·000
1·5	0·5	−0·746	0·431	−6·560	0·199	0·608	0·308	8·595	18·96	−0·957
1·5	1·0	−0·922	0·551	−5·704	0·186	0·563	0·285	9·681	20·07	−1·780
1·5	1·5	−1·190	0·688	−5·220	0·223	0·528	0·271	10·85	22·16	−2·502
1·5	2·0	−1·530	0·822	−5·138	0·310	0·517	0·255	12·00	24·94	−3·223
2·0	0·0	−0·643	0·428	−10·87	0·200	0·643	0·428	10·87	27·50	0·000
2·0	0·5	−0·742	0·515	−9·68	0·181	0·579	0·384	12.12	27·94	−1·278
2·0	1·0	−0·915	0·640	−8·66	0·169	0·513	0·368	13·48	29·55	−2·300
2·0	1·5	−1·168	0·796	−8·10	0·208	0·442	0·366	14·98	32·48	−2·972
2·0	2·0	−1·481	0·969	−7·98	0·298	0·377	0·365	16·56	36·17	−3·455
2·5	0·0	−0·637	0·486	−14·47	0·200	0·637	0·486	14·47	37·34	0·000
2·5	0·5	−0·746	0·579	−13·10	0·163	0·568	0·443	15·93	37·92	−1·635
2·5	1·0	−0·916	0·705	−11·98	0·151	0·490	0·433	17·55	40·08	−2·884
2·5	1·5	−1·159	0·870	−11·38	0·186	0·397	0·444	19·34	43·96	−3·501
2·5	2·0	−1·453	1·062	−11·29	0·269	0·304	0·457	21·20	48·63	−3·706
3·0	0·0	−0·638	0·533	−18·30	0·200	0·638	0·533	18·30	48·07	0·000
3·0	0·5	−0·755	0·632	−16·76	0·145	0·567	0·492	19·98	48·80	−2·068
3·0	1·0	−0·921	0·757	−15·57	0·135	0·482	0·487	21·86	51·58	−3·543
3·0	1·5	−1·157	0·925	−14·98	0·166	0·374	0·508	23·96	56·53	−4·106
3·0	2·0	−1·437	1·127	−14·98	0·243	0·259	0·536	26·11	62·25	−3·965

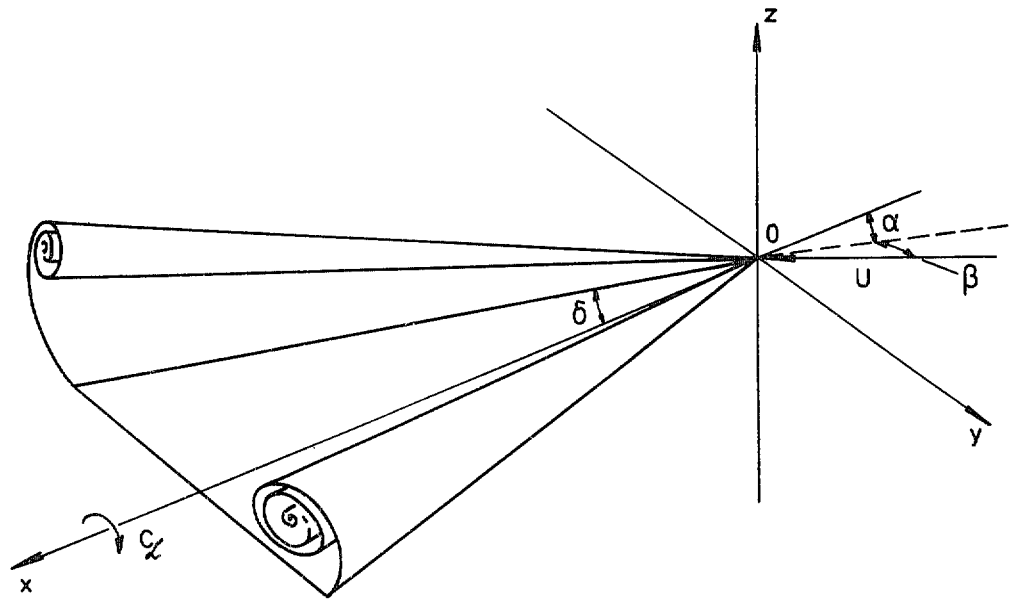

FIG. 1. Three-dimensional view of conical yawed flow past a slender delta wing with leading edge separation represented by vortex sheets.

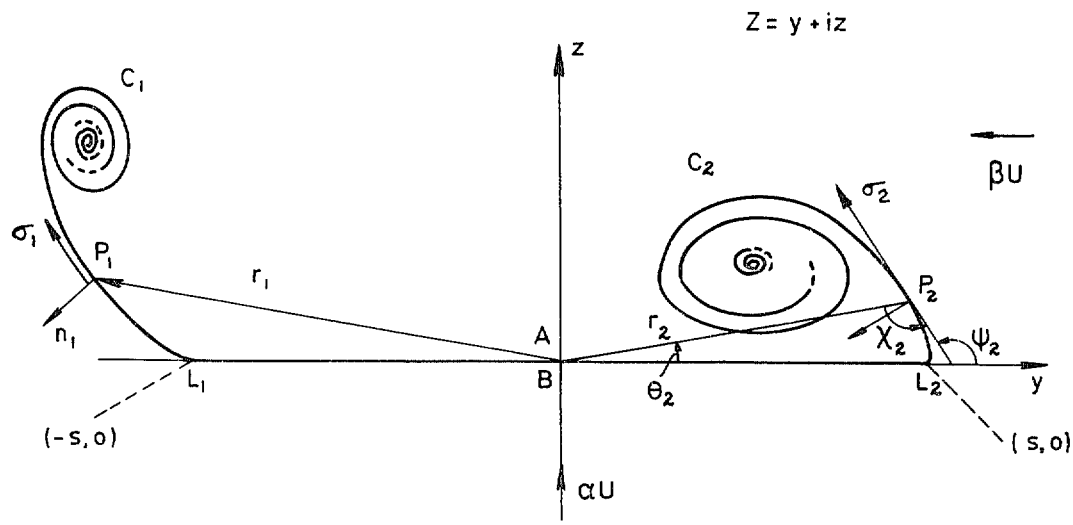

FIG. 2. Crossflow plane showing wing (L, AL_2B), leeward (C_1) and windward (C_2) vortex sheets.

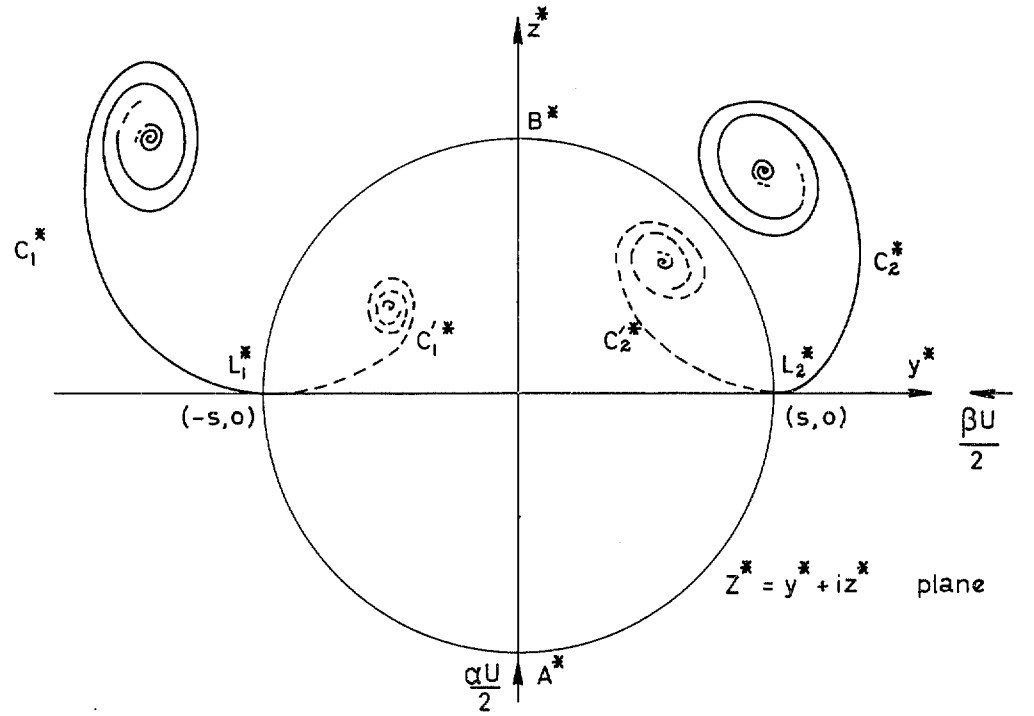

FIG. 3a. Vortex sheets in the transformed plane.

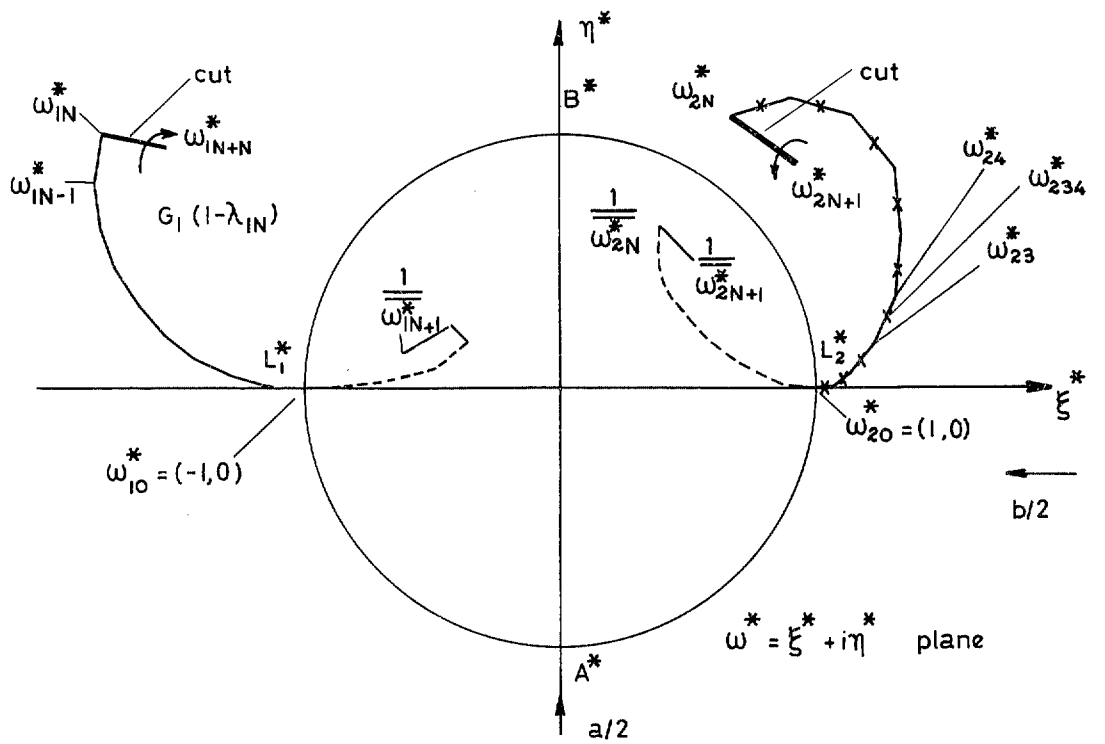

FIG. 3b. Breakup of vortex sheets for finite difference representation.

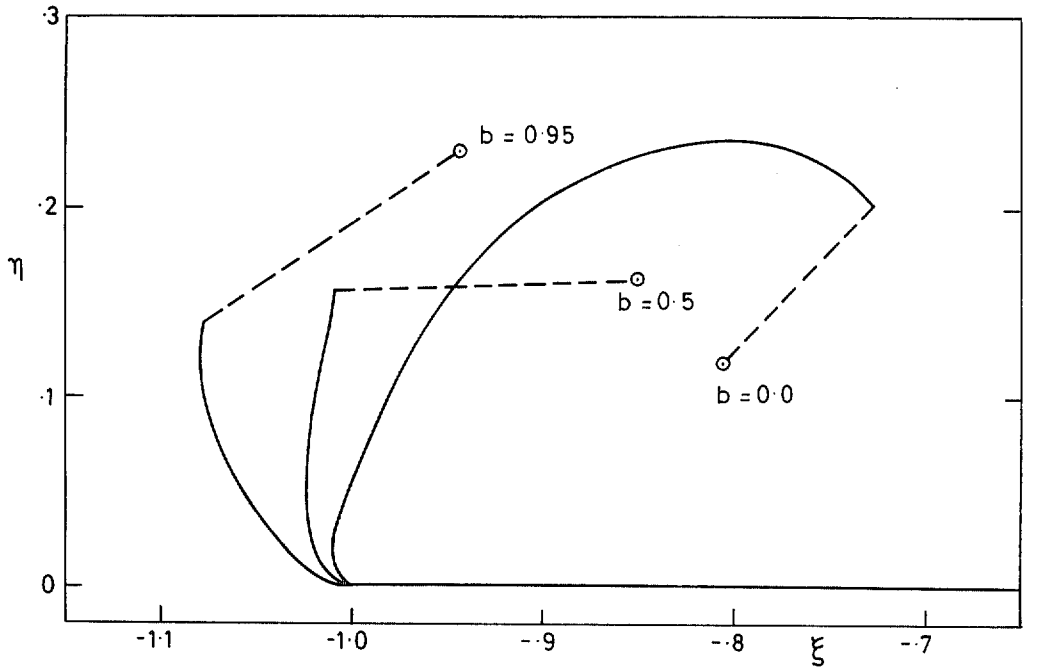

FIG. 4a. Leeward system; vortex sheet shape and position of isolated vortex for $a = 0{\cdot}5$, various b.

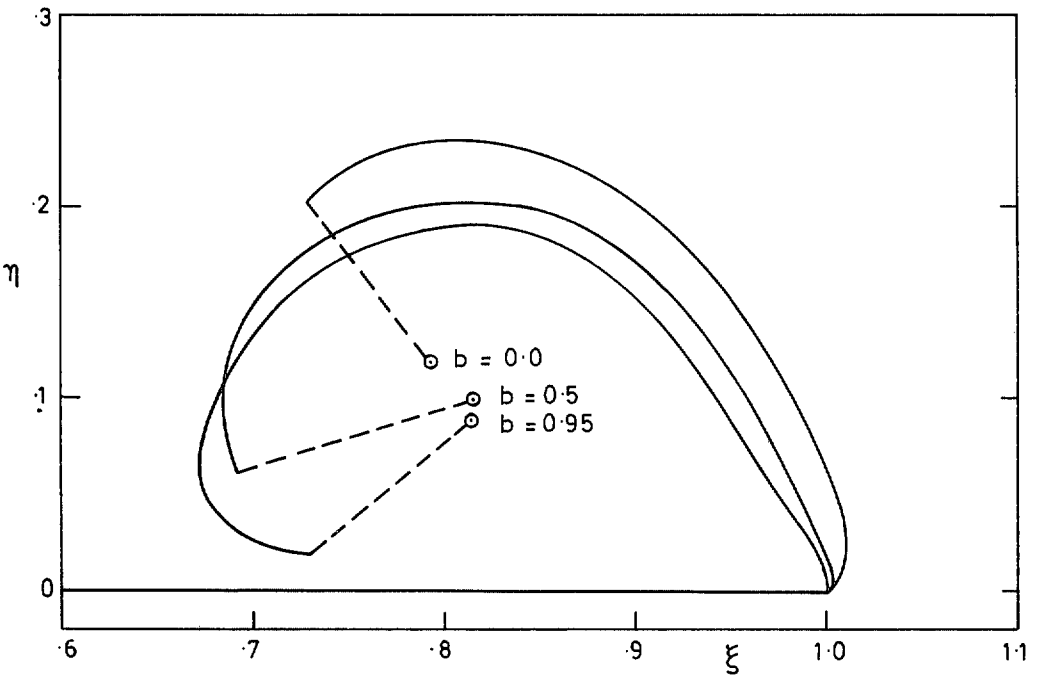

FIG. 4b. Windward system; vortex sheet shape and position of isolated vortex for $a = 0{\cdot}5$, various b.

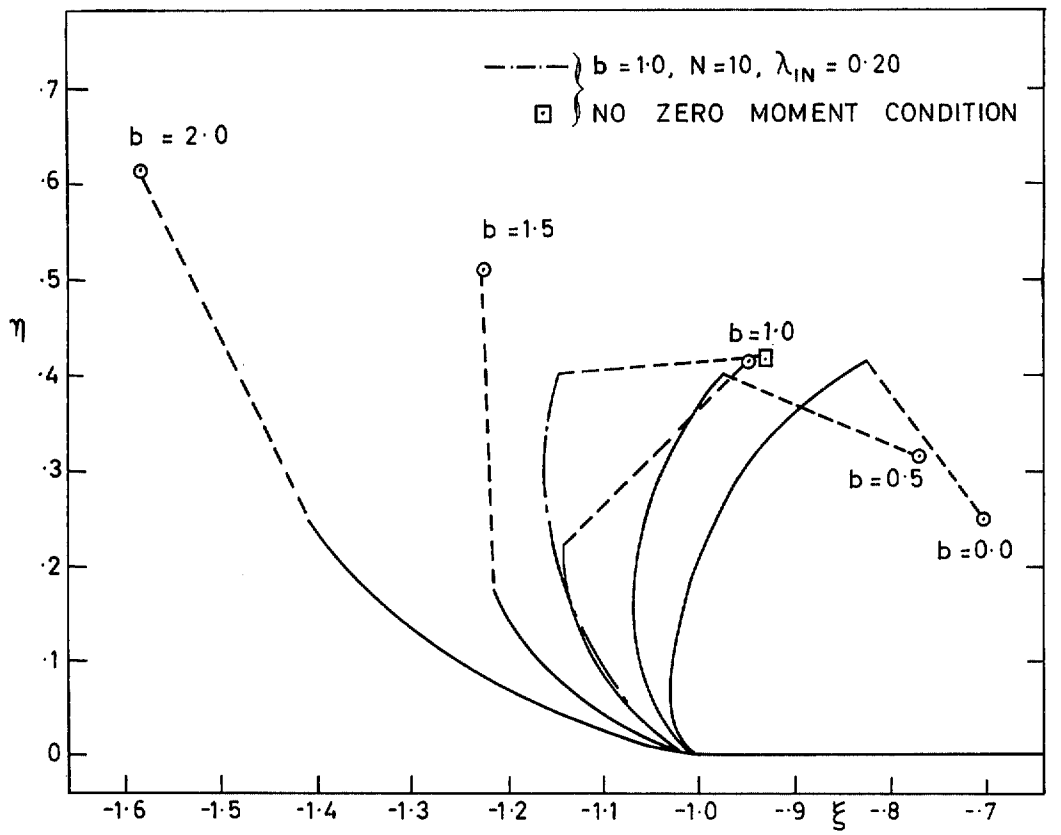

FIG. 5a. Leeward system; vortex sheet shape and position of isolated vortex for $a = 1{\cdot}0$, various b.

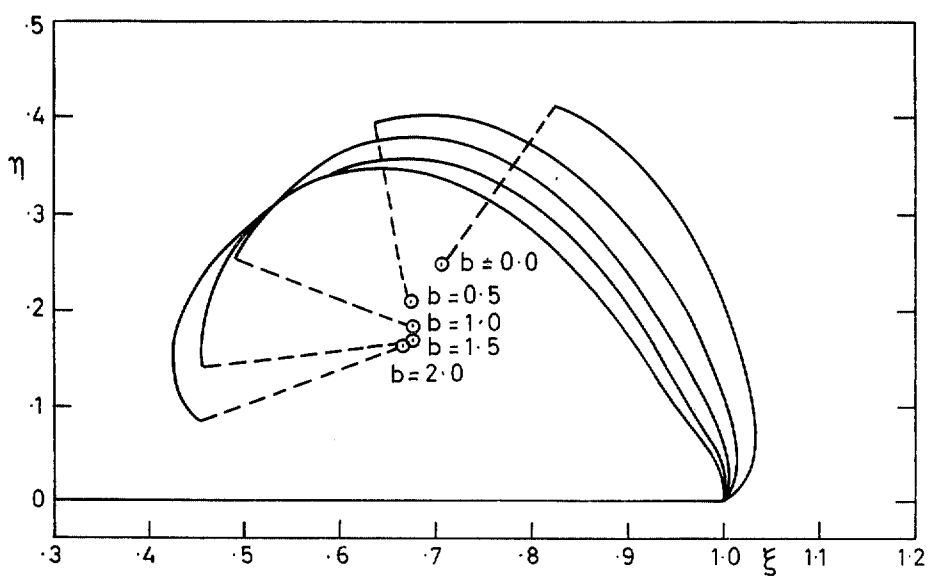

FIG. 5b. Windward system; vortex sheet shape and position of isolated vortex for $a = 1{\cdot}0$, various b.

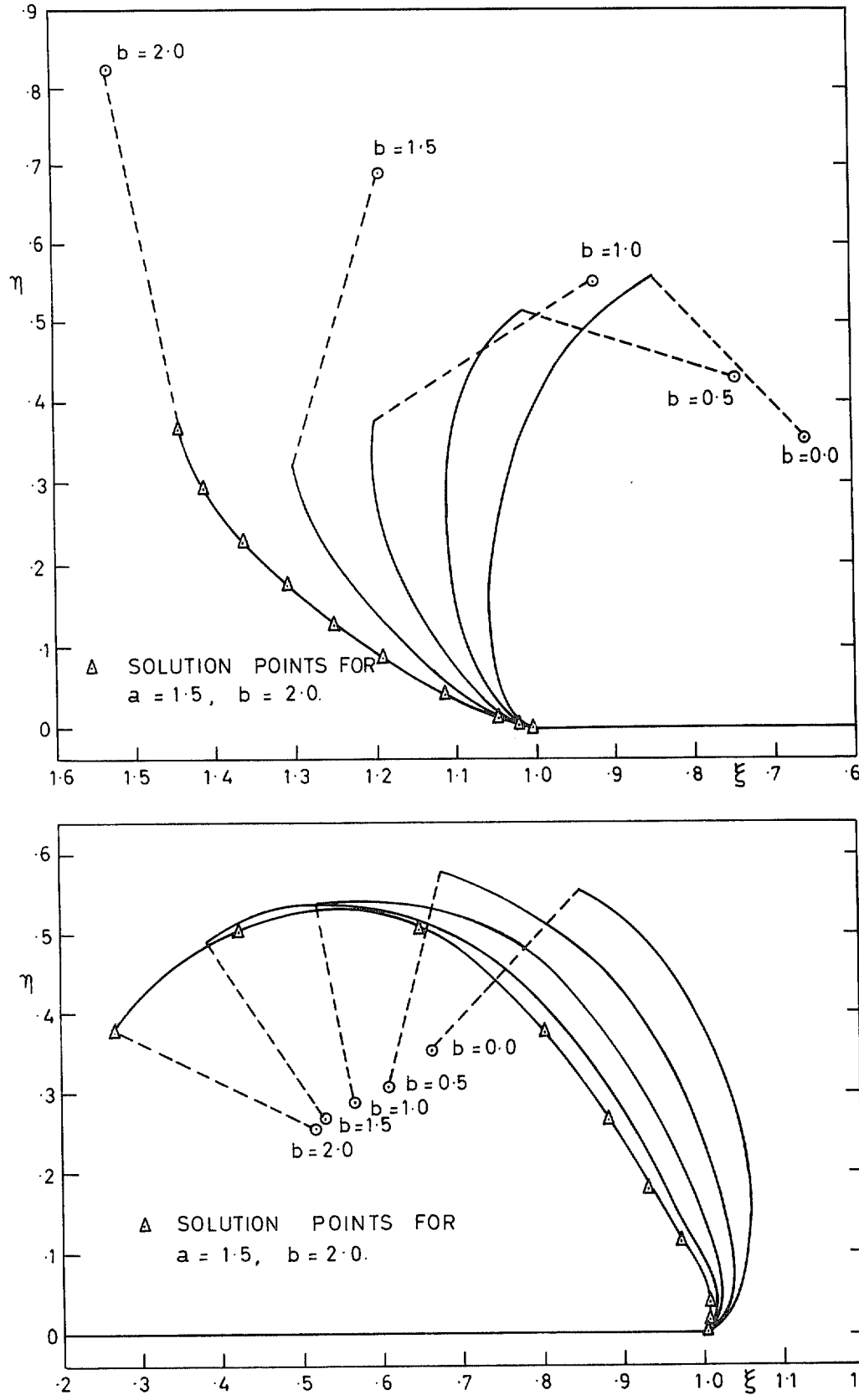

FIGS. 6a Top (leeward system) and 6b bottom (windward system) vortex sheet shape and position of isolated vortex for $a = 1{\cdot}5$, various b.

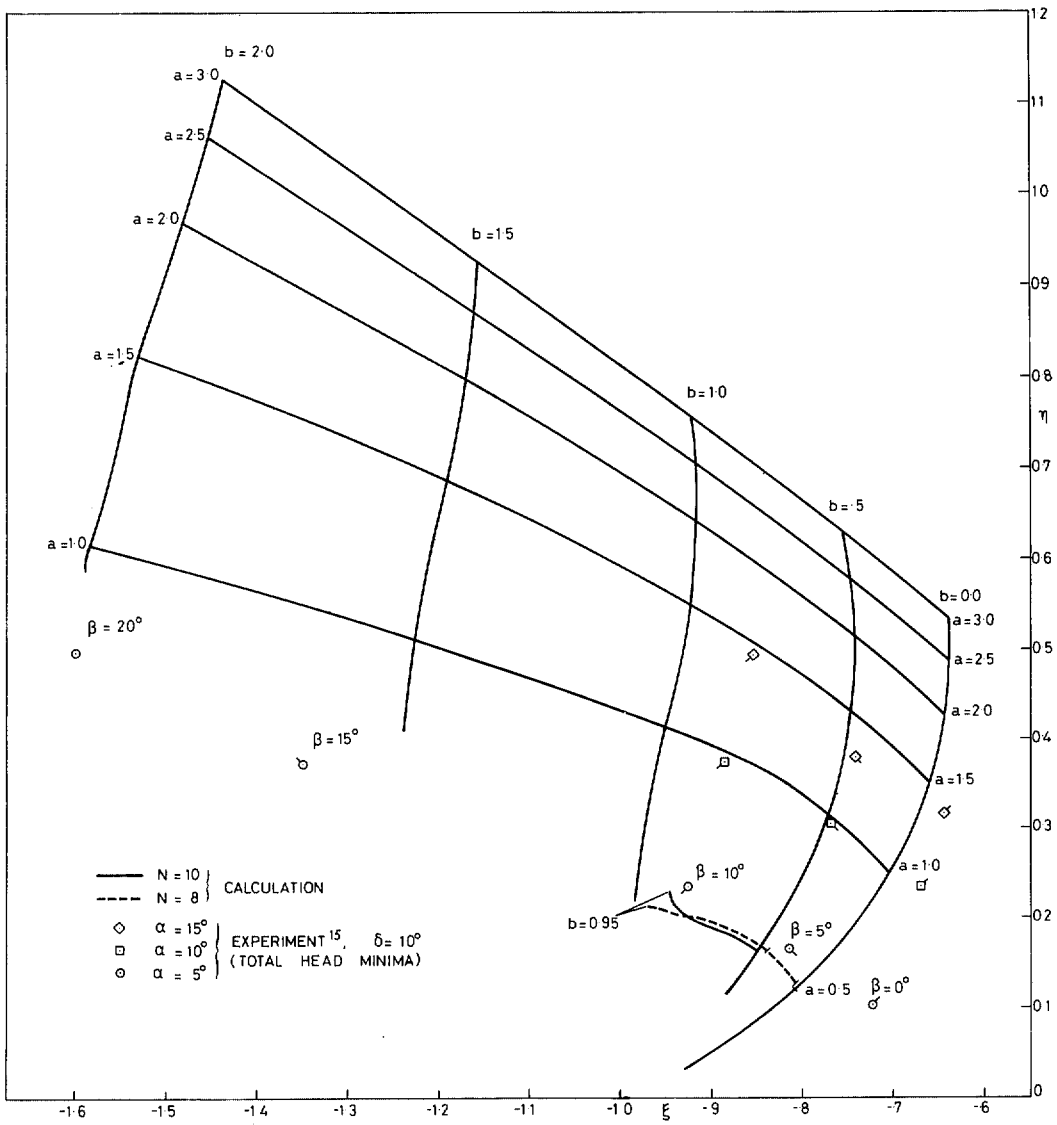

FIG. 7. Variation of calculated and measured position of leeward vortex with incidence and yaw.

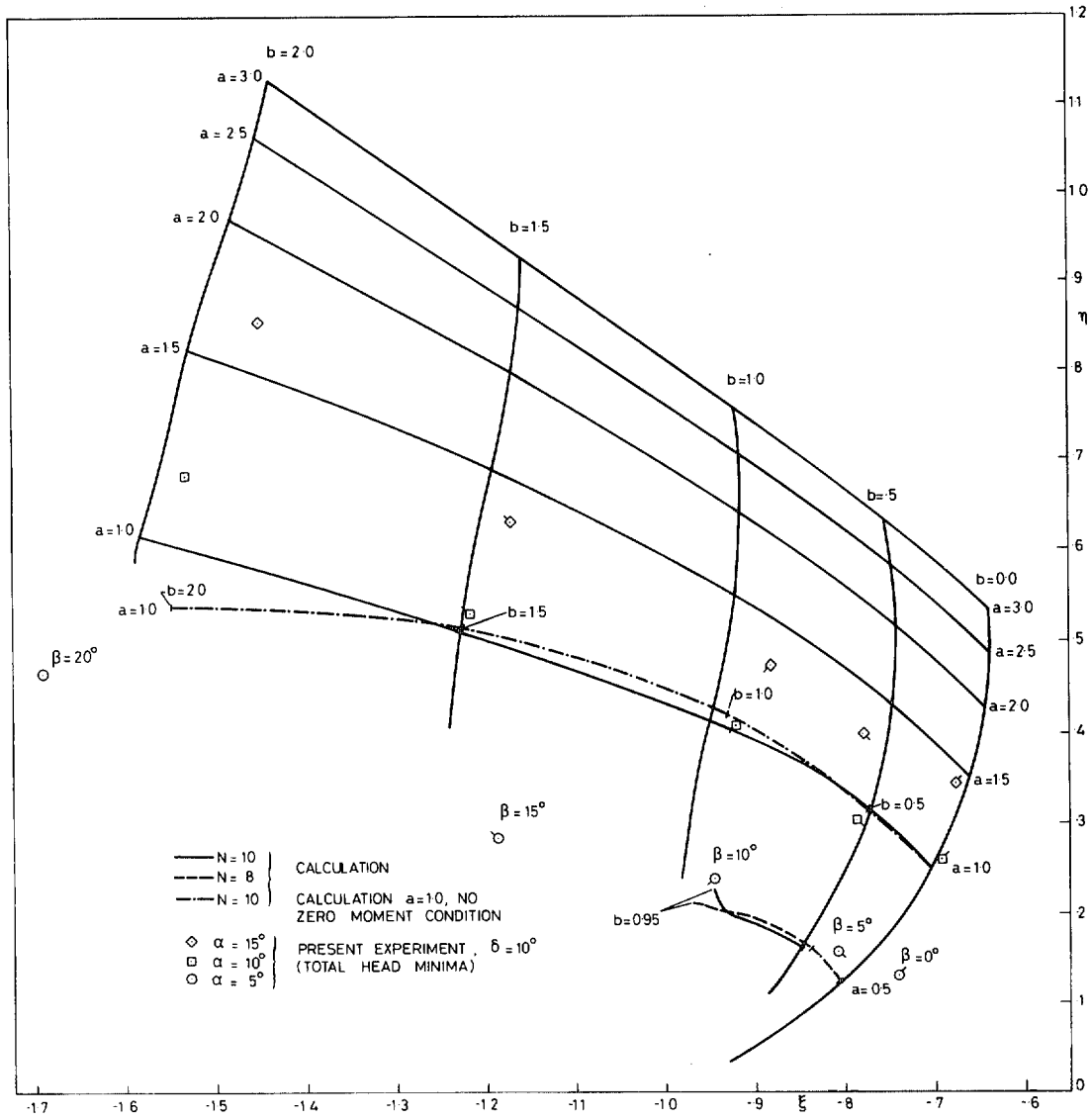

FIG. 8. Variation of calculated and measured position of leeward vortex with incidence and yaw.

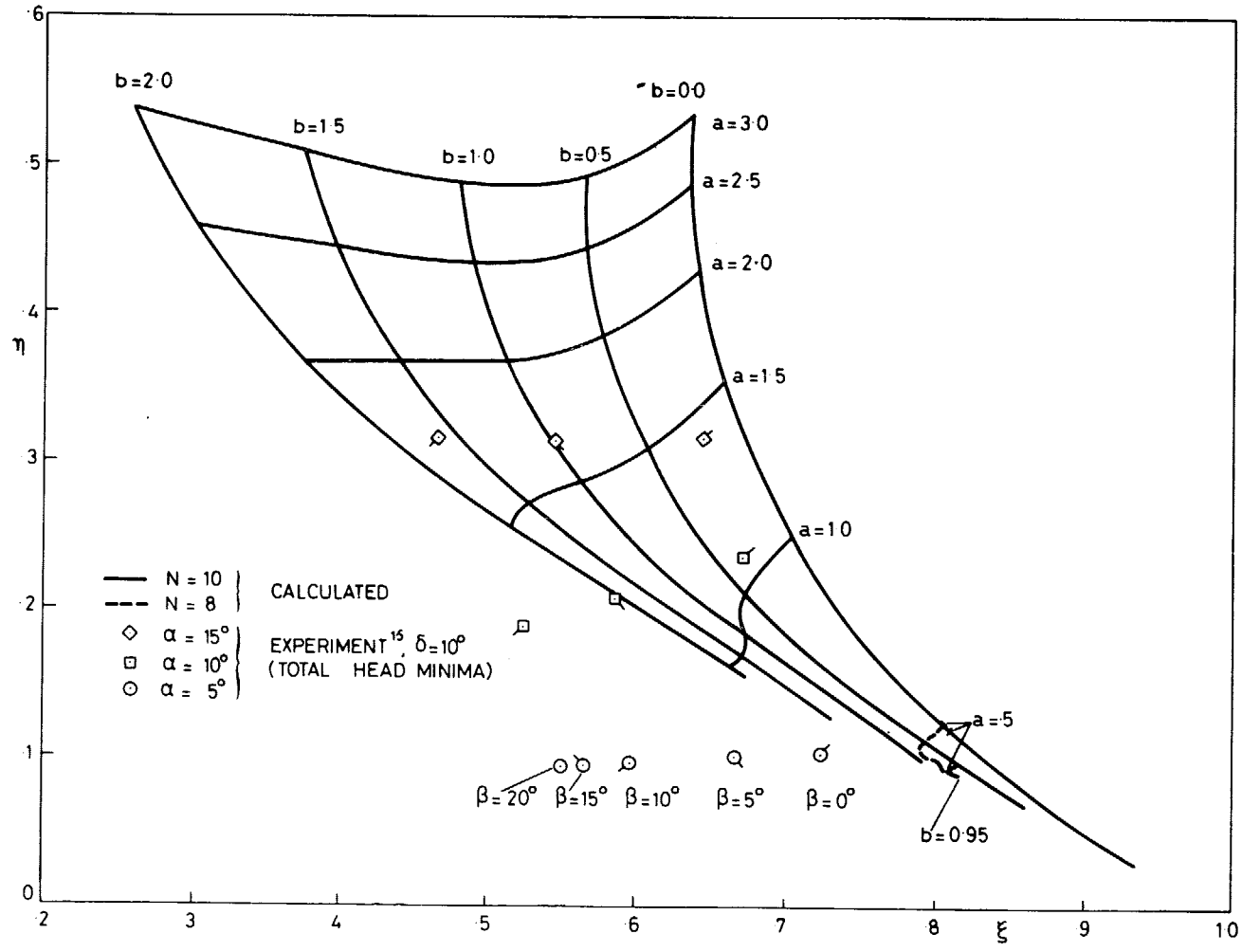

FIG. 9. Variation of calculated and measured position of windward vortex with incidence and yaw.

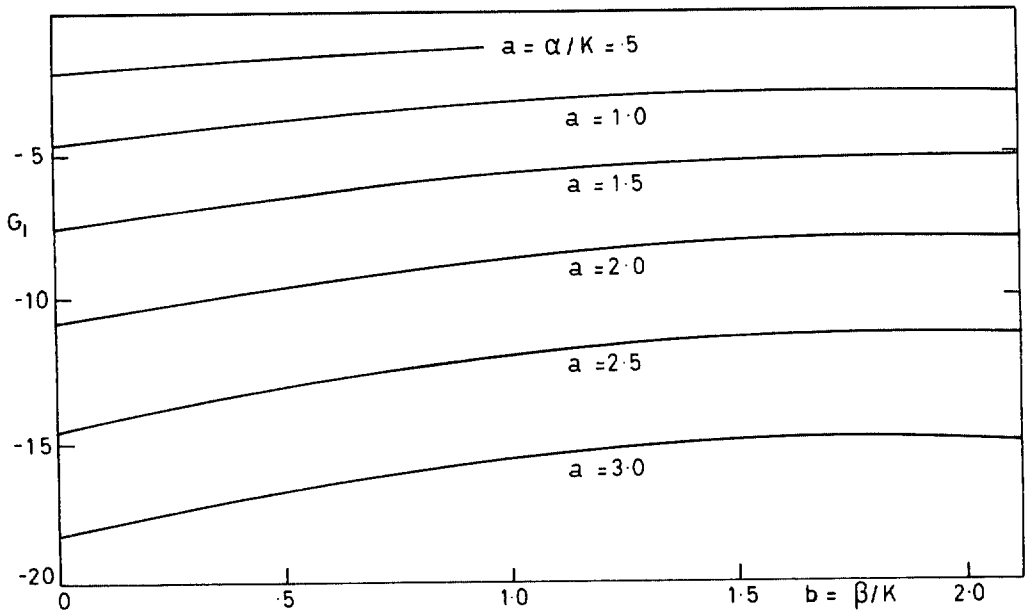

FIG. 10a. Variation of total circulation, $G_1 = \Gamma_{r_1}/KUs$ of leeward sheet + vortex, with b for various a.

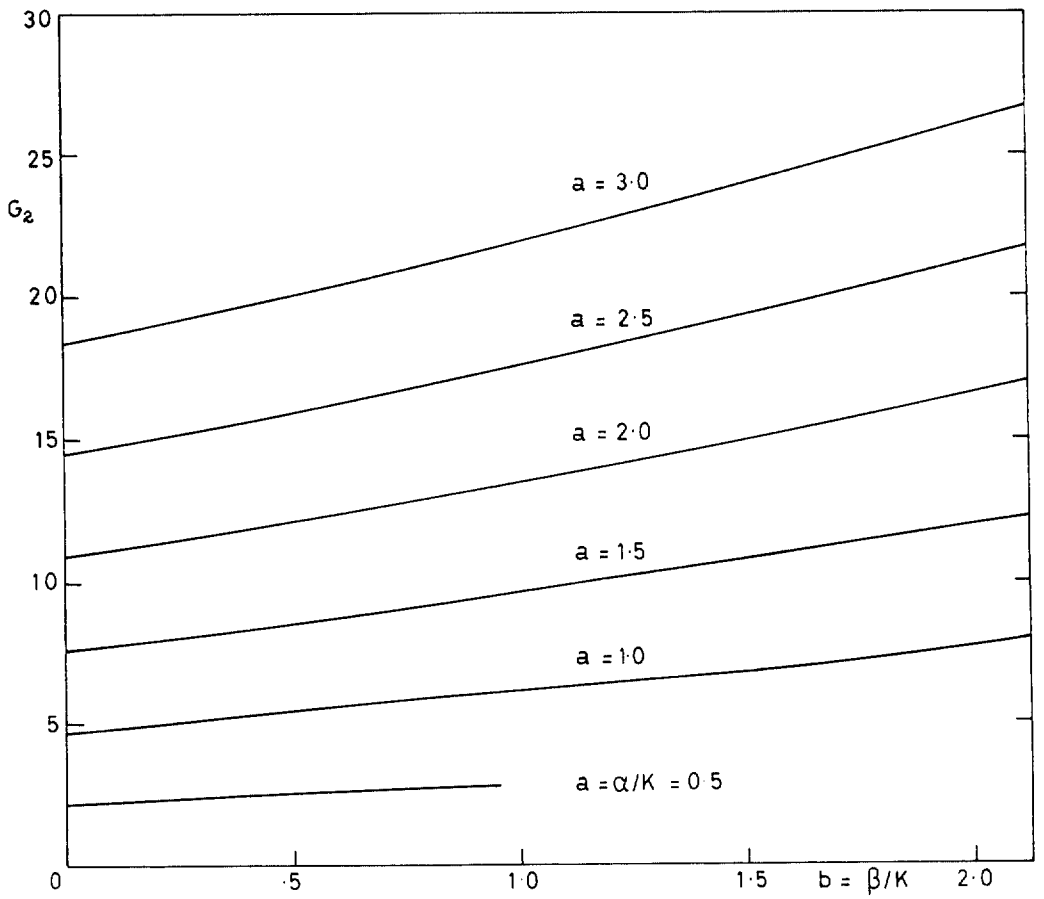

FIG. 10b. Variation of total circulation, $G_2 = \Gamma_2/KUs$ of windward sheet + vortex with b for various a.

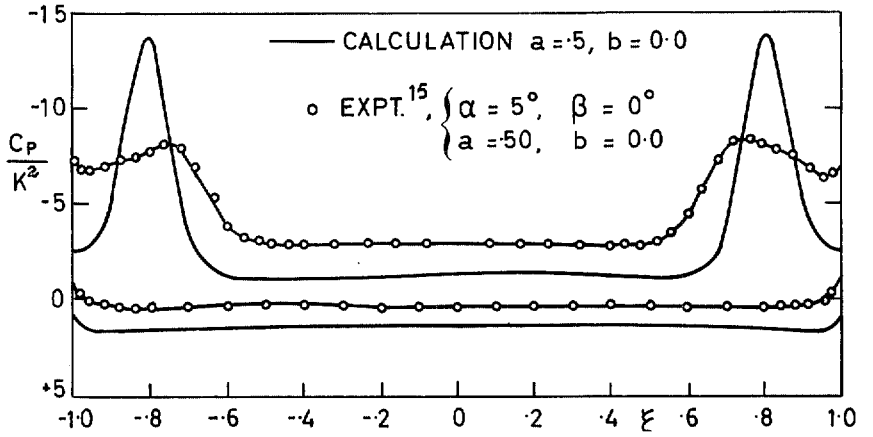

FIG. 11a.

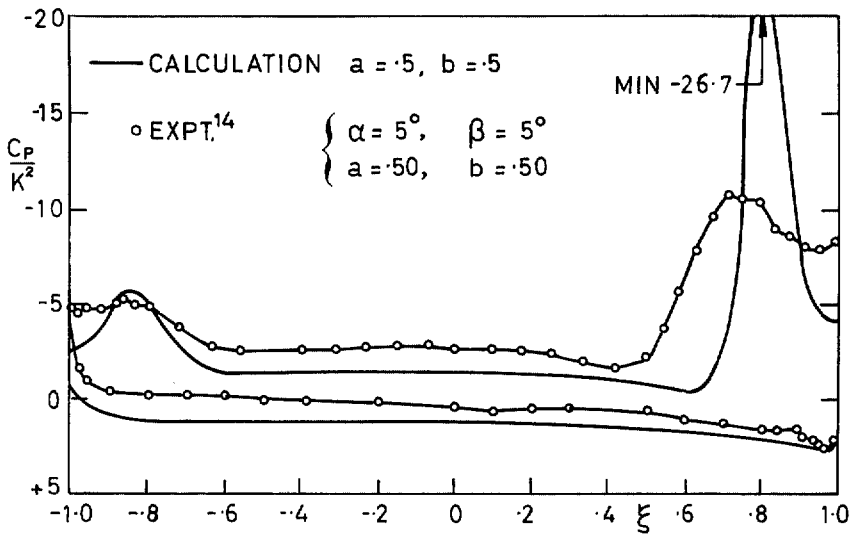

FIG. 11b.

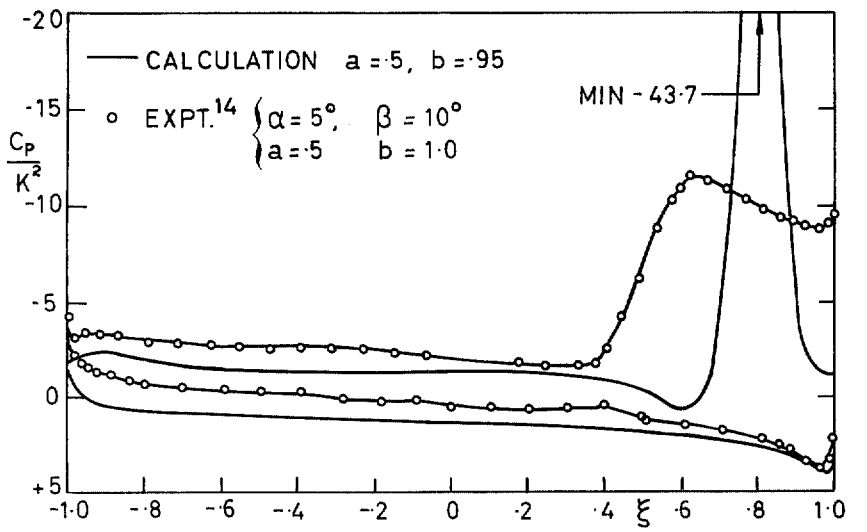

FIGS. 11a, 11b, & 11c. Pressure on wing upper and lower surface $a = 0{\cdot}5$.

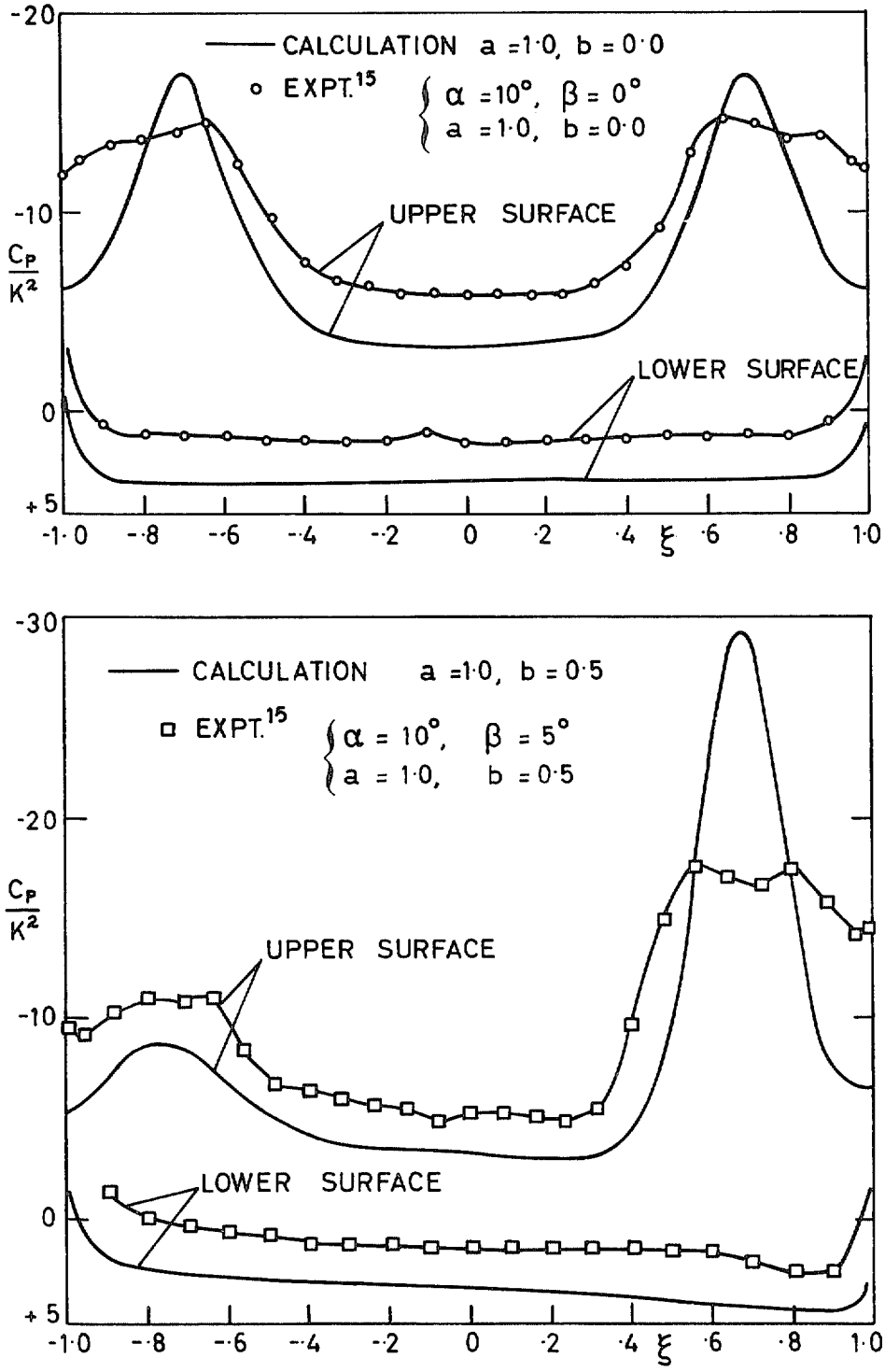

FIGS. 12a & 12b. Pressure on wing upper and lower surface $a = 1{\cdot}0$.

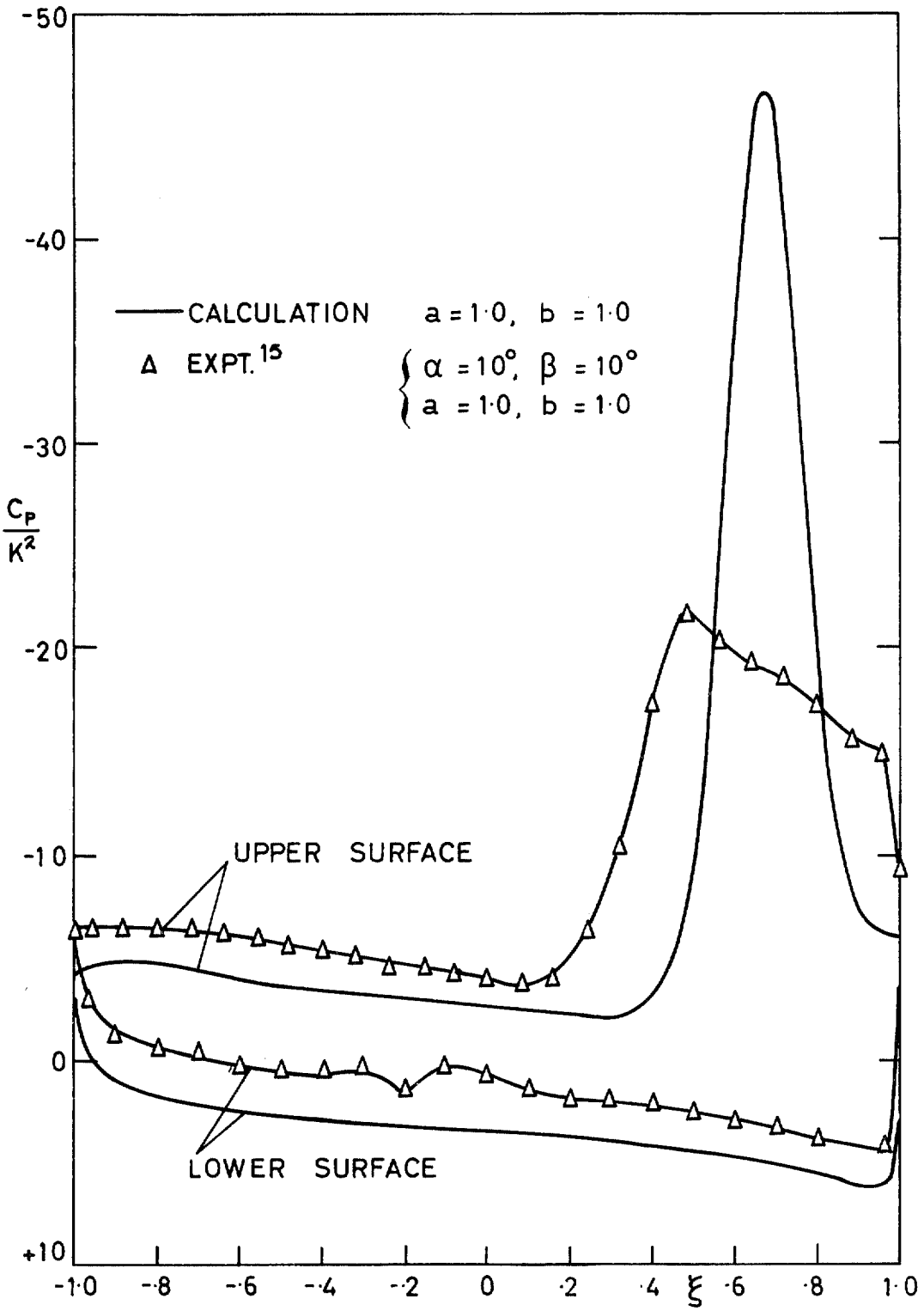

FIG. 13. Pressure on wing upper and lower surface.

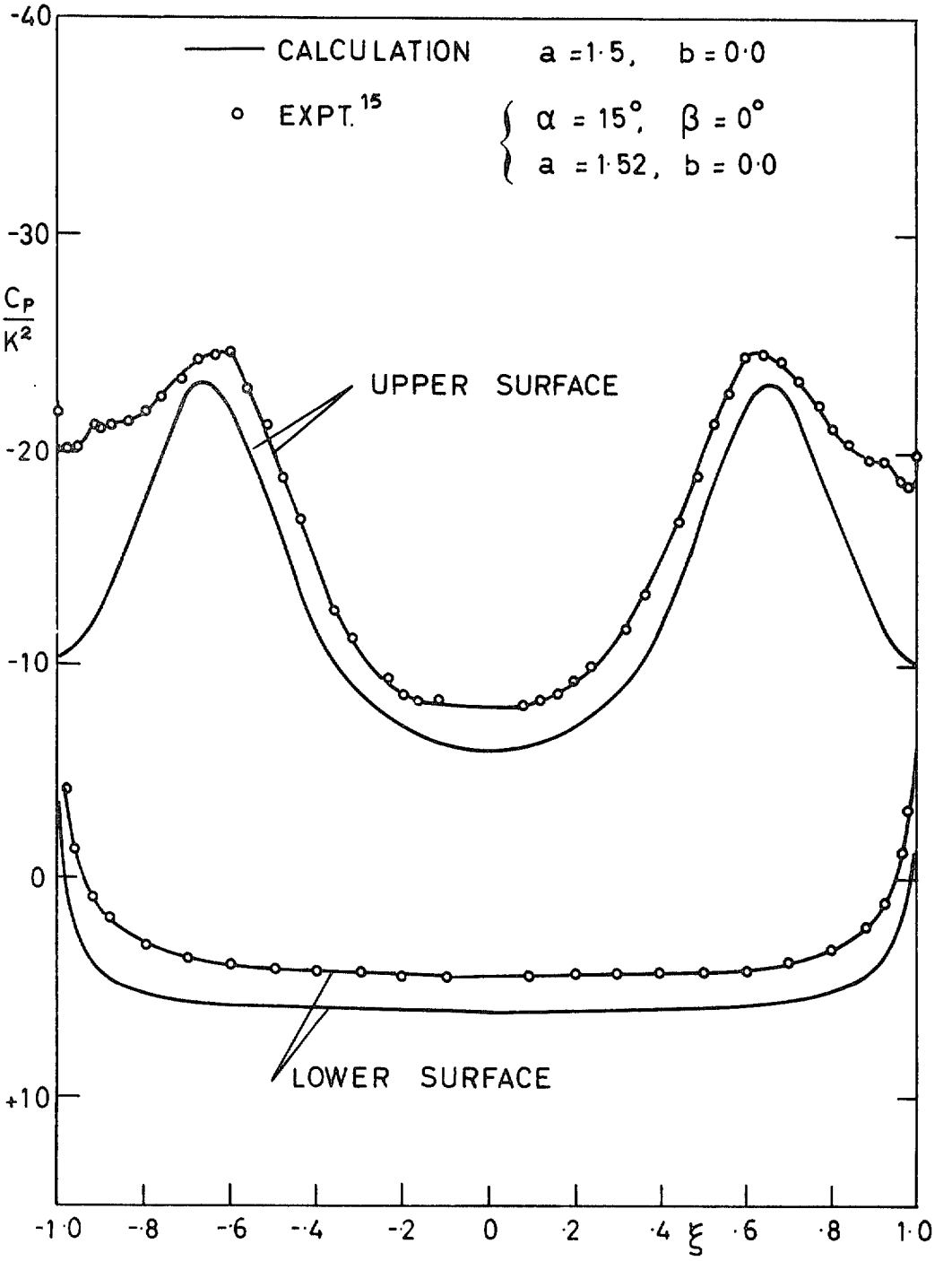

FIG. 14. Pressure on wing upper and lower surface.

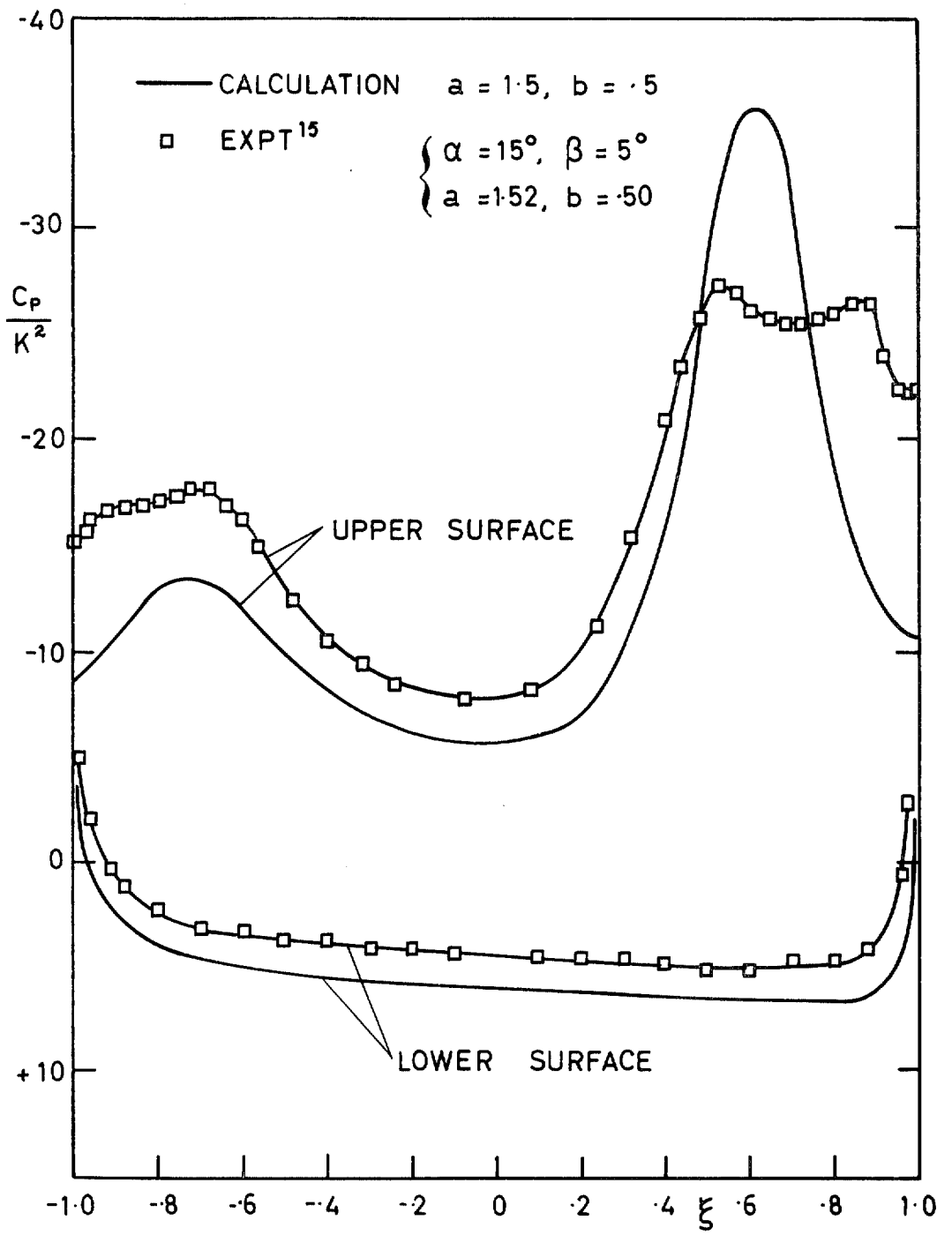

FIG. 15. Pressure on wing upper and lower surface.

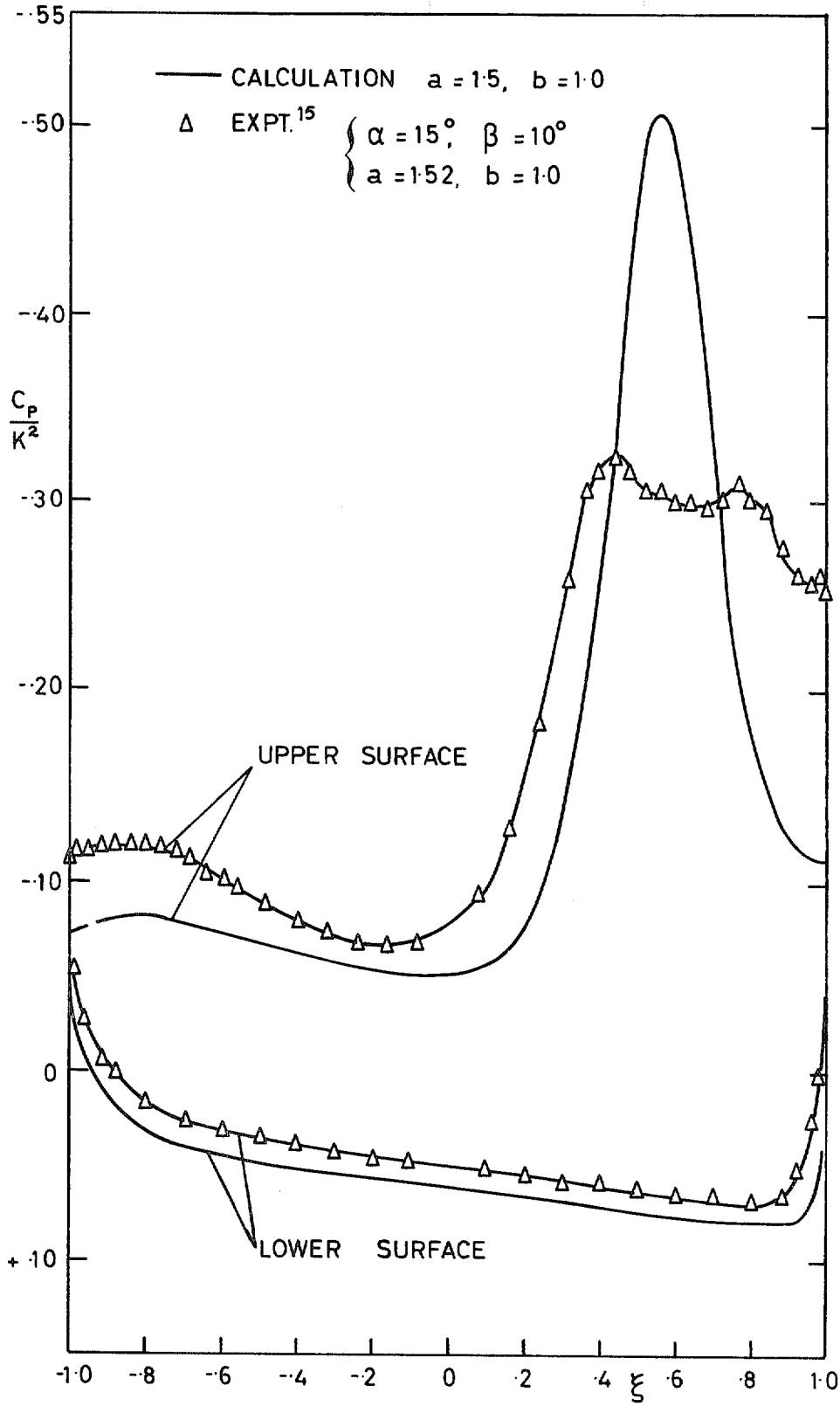

FIG. 16. Pressure on wing upper and lower surface.

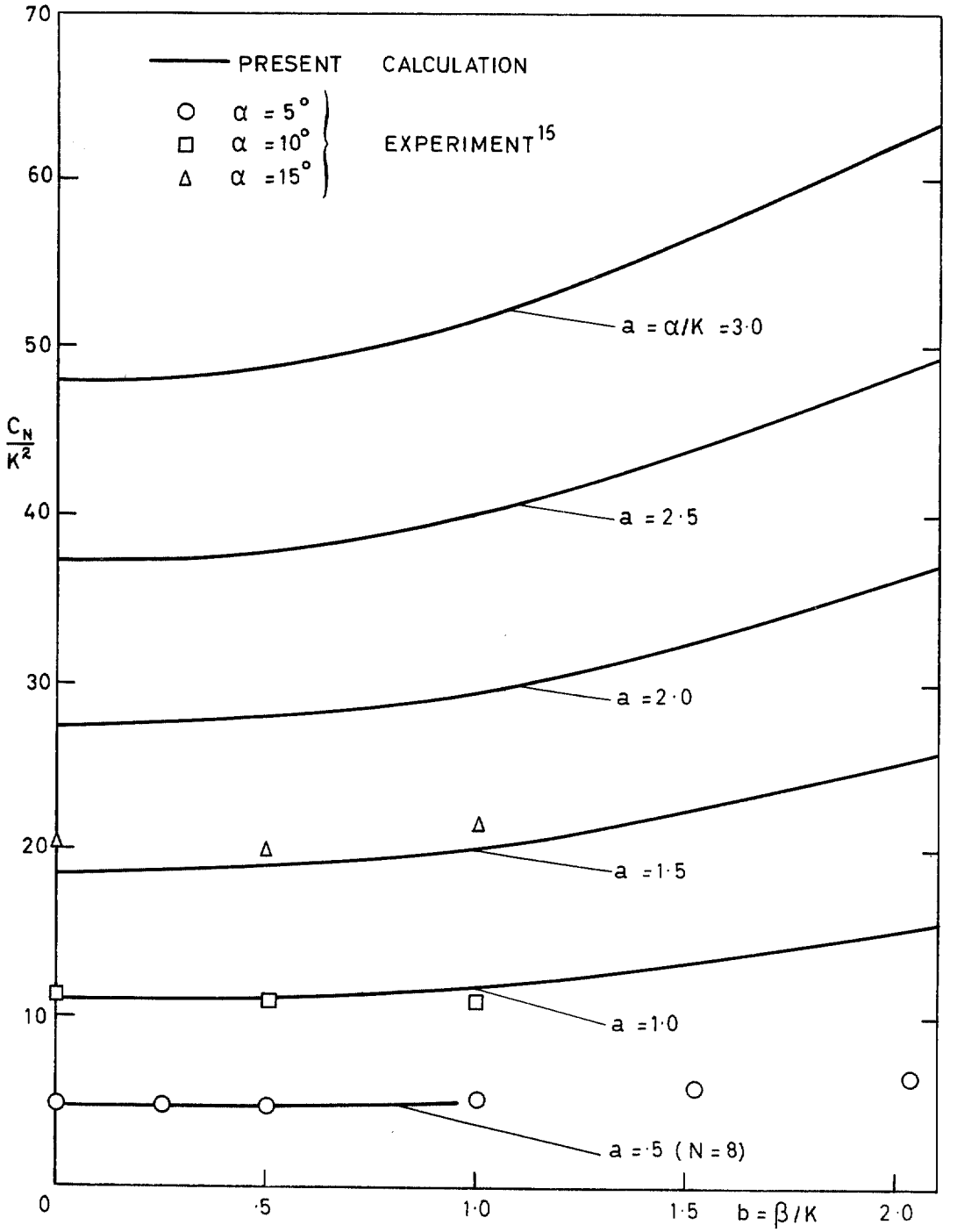

FIG. 17. Variation of lift coefficient with b for various a.

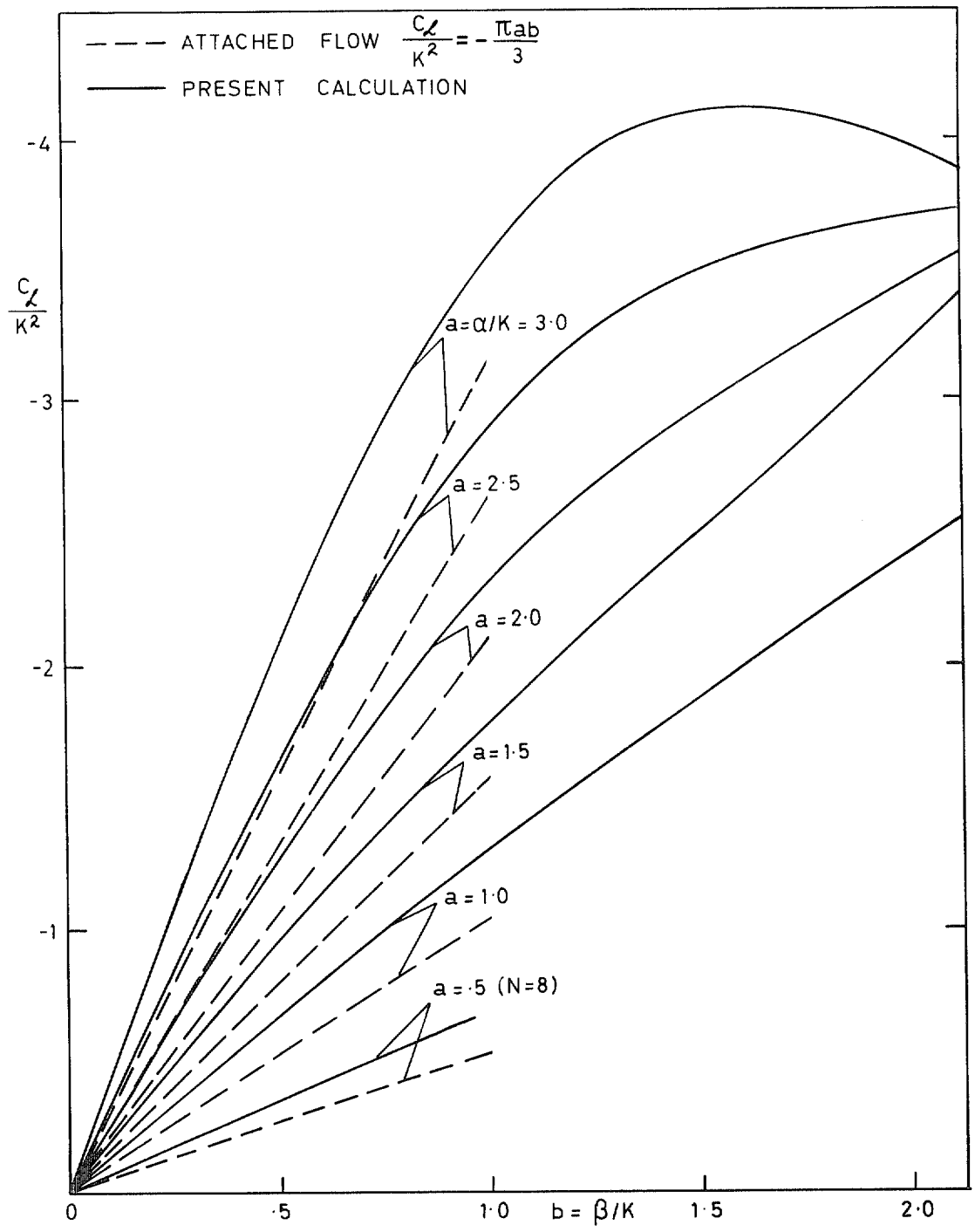

FIG. 18. Variation of rolling moment coefficient with b for various a.

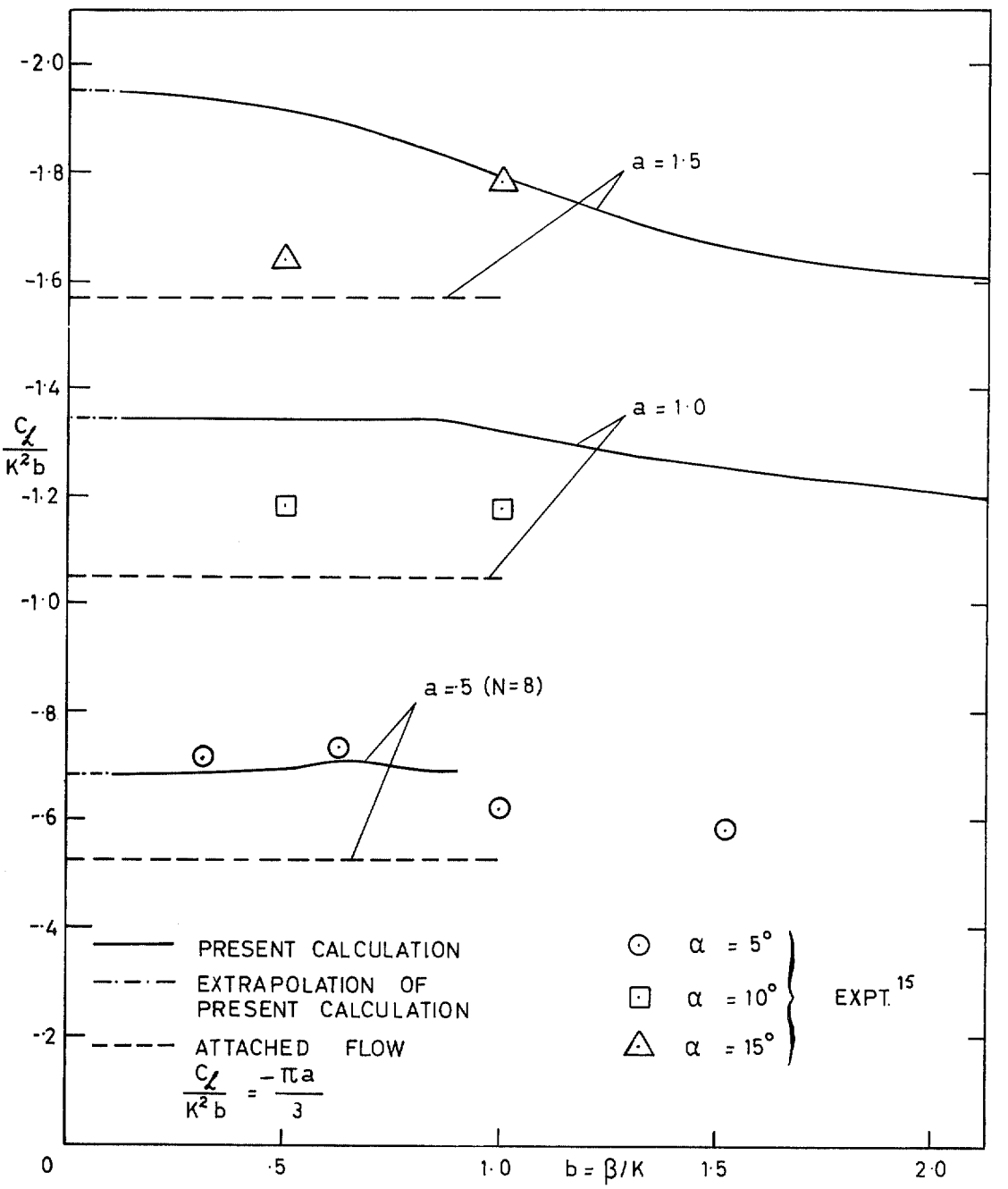

FIG. 19. Variation of rolling moment coefficient plotted as $C_\ell/(K^2 b)$, with b for various a.

Printed in England for Her Majesty's Stationery Office by J. W. Arrowsmith Ltd., Bristol BS3 2NT
Dd. 505374 K5 5/75

HER MAJESTY'S STATIONERY OFFICE

Government Bookshops

49 High Holborn, London WC1V 6HB
13a Castle Street, Edinburgh EH2 3AR
41 The Hayes, Cardiff CF1 1JW
Brazennose Street, Manchester M60 8AS
Southey House, Wine Street, Bristol BS1 2BQ
258 Broad Street, Birmingham B1 2HE
80 Chichester Street, Belfast BT1 4JY

Government Publications are also available through booksellers

ISBN 0 11 470912 2